

**Evaluation of Radiometric and Polarimetric Calibration of  
Airborne L-band Full-Pol data**



**December- 2019**

**Calibration and Validation Division**

**Earth, Ocean, Atmosphere, Planetary Sciences & Application Area**

**Space Application Center (ISRO)**

**Ahmedabad - 380 015**

## DOCUMENT CONTROL SHEET

1. Report No.	SAC/EPESA/CVD/CAL-VAL/SR/01/12/2019
2. Publication date	December -2019
3. Title and subtitle	Evaluation of Radiometric and Polarimetric Calibration of Airborne L-band Full-Pol data
4. Type of report	Scientific
5. Number of pages	64
6. Authors	CAL-VAL Team
7. Originating unit	CVD- EPESA
8. Abstract	<p>Development of NASA-ISRO Dual frequency SweepSAR (NISAR) is under progress by ISRO in collaboration with Jet Propulsion Laboratory (JPL), NASA. It will provide S- and L-band space-borne SAR data with high repeat cycle, high resolution, and larger swath, with capability of full-polarimetric and Interferometric modes of operation. For the quantitative interpretation of images, acquired by SAR sensor, it is very much important to have properly calibrated data. Due to limited number of datasets available for ISRO's L&amp;S airborne SAR mission (pre-cursor to NISAR), full-pol data of UAVSAR is used in this study to derive the polarimetric distortion matrix (PDM) and validate the results. In this report, results of the evaluation of the radiometric and polarimetric calibration of UAVSAR L-band data using point targets and distributed target are presented. Analysis of the impulse response function of the targets show that the estimated azimuth resolution (<math>0.93 \pm 0.02</math> meters) and range resolution (<math>2.69 \pm 0.06</math> meters) are close to the specified values. The difference between the estimated and provided calibration constant was found to be in the range of <math>1 \text{ dB} \pm 0.45 \text{ dB}</math> with a phase calibration error of <math>1.58^\circ</math>. Co-polarization channel imbalance (f) was found to be <math>0.985 \pm 0.052</math> (linear units), which is estimated using corner reflectors.</p>

	<p>While cross polarization channel imbalance (g) was calculated as 1.256 dB which is derived using featureless homogenous area (distributed target). The phase anomaly between cross channel of HV and VH polarization was found to be <math>-2.07^\circ</math>, which indicates that the phase error is high in receiving channel. The undulations present in the polarimetric signatures of co-pol and cross-pol after radiometric and phase correction, indicates that cross talk and channel imbalances are present. Polarimetric signature was also derived for point targets using polarimetric calibrated images and are shown in this report. Estimation of polarimetric distortion matrix (PDM) was done using advanced and robust Quegan's algorithm. Application of estimated PDM to the radiometrically and phase corrected dataset is in progress to validate the results. Once validated, this will be used to carry out the polarimetric calibration of ISRO's L&amp;S airborne SAR and NISAR full-pol data.</p>
9. Key words	Radiometric and Phase calibration, Polarimetric calibration, cross talk, channel imbalance, SAR calibration, UAVSAR
10. Security classification	Unrestricted
11. Distribution statement	General

## **CAL-VAL Team**

### **1. Space Applications Centre (SAC-ISRO), Ahmedabad**

Mrs. Shweta Sharma- Principal Investigator

Mr. Saurabh Tripathi- Co-Principal Investigator

Dr. A K Mathur- Ex-Head, CVD/EPISA

### **2. Nirma University, Ahmedabad**

Dr. P R Patel- Co-Principal Investigator

Mr. B. Sowkhya- Junior Research Fellow (JRF)

## Table of Contents

I.	List of Figures.....	7
II.	List of Tables.....	8
1	INTRODUCTION .....	9
2	OBJECTIVES.....	11
3	STUDY AREA .....	12
4	DATA USED.....	13
4.1	POLARIMETRIC TARGET DESCRIPTIONS .....	15
4.1.1	<i>Scattering Matrix (S)</i> .....	15
4.1.2	Covariance (C) and Coherency (T) Matrices.....	17
5	METHODOLOGY .....	19
5.1	Radiometric and Phase Calibration.....	19
5.1.1	<i>Estimation of Absolute Calibration Parameter (A):</i> .....	20
5.1.2	<i>Estimation of co-pol channel imbalance (f) and phase difference <math>\phi_t</math></i> .....	21
5.1.3	<i>Estimation of cross-pol channel imbalance (g) and phase difference <math>\phi_r</math></i> .....	22
5.2	Polarimetric Calibration.....	22
5.2.1	<i>Distortion Models</i> .....	23
5.2.2	<i>Polarimetric signatures</i> .....	25
6	RESULTS AND DISCUSSIONS.....	26
6.1	Radiometric and Phase Parameters .....	26
6.1.1	<i>Impulse Response Functions for HH polarization</i> .....	31

6.1.2	<i>Impulse Response Functions for VV polarization</i> .....	35
6.1.3	<i>Channel Imbalance and Phase Bias</i> .....	38
6.1.4	<i>Polarimetric signatures after radiometric and phase correction</i> .....	40
6.2	Polarization parameters .....	45
6.2.1	<i>Impulse Response Function for HV polarization</i> .....	45
6.2.2	<i>Estimation of cross talk and channel imbalance by Quegan's Method</i> .....	50
6.3	Polarimetric Signatures- GRD Data.....	51
6.4	Opportunistic Targets- Windmills present in the UAVSAR L band SLC data .....	56
7	SUMMARY AND CONCLUSIONS .....	62
	ACKNOWLEDGEMENTS.....	63
	REFERENCES .....	63

## I. List of Figures

Figure 1. Local incidence angle ( $\eta$ ) and look angle ( $\gamma$ ) of airborne SAR assuming flat earth ...	11
Figure 2. UAVSAR/Gulfstream-III at an airport. UAVSAR Antenna is contained in the pod mounted under the GIII body .....	11
Figure 3. Google Earth image showing study area footprint (left image) and display of deployed corner reflectors at Rosamond dry lake bed (right image) .....	12
Figure 4. 2.4-meter trihedral triangular corner reflector .....	13
Figure 5. SLC image of HH-pol showing corner reflectors deployed at Rosamond dry lake.....	15
Figure 6. Graph showing RCS difference for HH and VV pol. ....	28
Figure 7. Graph showing peak power values for HH and VV pol. in linear amplitude units.....	28
Figure 8. Graph showing peak power difference between HH and VV pol. in linear amplitude units .....	29
Figure 9. Graph showing phase difference HH-VV pol.....	30
Figure 10. Location of CR's in SLC image of HH pol .....	31
Figure 11. Impulse Response function of CR's using SLC image of HH pol.....	34
Figure 12. Impulse Response function of CR's using SLC image of VV pol.....	37
Figure 13. Polarimetric Signature of corner reflector in ideal case: Co-polarization signature of corner reflector before radiometric and phase calibration (left image); Co-polarization signature of corner reflector after radiometric and phase calibration (right image); ©(Alexander, Bruce and Brian 2014) .....	40
Figure 14. Polarimetric Signatures of Triangular Trihedral Corner Reflector after Radiometric and Phase Calibration.....	45
Figure 15. Location of CR's in SLC image of HV pol.....	46
Figure 16. Impulse Response of CR using SLC image of HV .....	49
Figure 17. Polarimetric signature of triangular trihedral corner reflector (ideal case) © (Abhisek, Shashi and Valentyn 2019) .....	51

<b>Figure 18. polarimetric signatures of each CR after cross talk and channel imbalance calibration .....</b>	<b>55</b>
<b>Figure 19. Above fig. are SLC (left); MLC (right) tile of UAVSAR L band data showing windmills .....</b>	<b>56</b>
<b>Figure 20. showing windmills in Google Earth image .....</b>	<b>56</b>
<b>Figure 21. Impulse response function of windmills using SLC HH pol. data.....</b>	<b>61</b>

## II. List of Tables

<b>Table 1. List of precision data files and radar parameters of SLC imagery .....</b>	<b>13</b>
<b>Table 2. List of precision data files and radar parameters of Multilook imagery .....</b>	<b>14</b>
<b>Table 3. Attributes used to calculate RCS of each CR with respect to Incidence and Azimuth angle.....</b>	<b>26</b>
<b>Table 4. Details of clutter and deviation of RCS from theoretical value .....</b>	<b>27</b>
<b>Table 5. Range and Azimuth resolution estimated from IRF of the point targets.....</b>	<b>30</b>
<b>Table 6. Calculated Target Energy values after subtraction of clutter for quad pol.....</b>	<b>38</b>
<b>Table 7. Estimation of co channel imbalance (f) .....</b>	<b>38</b>
<b>Table 8. Estimation of cross channel imbalance (g).....</b>	<b>39</b>
<b>Table 9. Estimated Phase bias in transmitter and receiver for co-pol and cross-pol channels....</b>	<b>40</b>
<b>Table 10. Estimation of cross talk and channel imbalance using Quegan algorithm .....</b>	<b>50</b>
<b>Table 11 Range and Azimuth resolution at 3dB width using opportunistic targets (windmills)..</b>	<b>57</b>

# **1 INTRODUCTION**

Synthetic Aperture Radar (SAR) is a progressive remote sensing technology used to retrieve the characteristics of Earth's surface targets, which also has capabilities to acquire the data during all weather conditions, day and night imaging capability. SAR is an active microwave radar system, transmitting horizontal or vertical polarized signals towards the target and receives backscattered energy from the target. Single pol radar system transmits the horizontal (HH) or vertical (VV) polarization signal and receives the signal in the same polarization. In case of dual pol or full pol radar system, it transmits the signal in both the polarization channels alternatively but receives the signal from the target in both the polarization channels simultaneously. In hybrid pol radar system, circular polarized pulse either left or right circular signal is transmitted in horizontal or vertical direction, and backscatter is received in both the polarized channels. These unique microwave radar polarization systems i.e., linear polarization, circular polarization, etc., helps in retrieving additional information about the target.

The Polarimetric radar data gives amplitude and phase information from the behaviour of the scattered waves from a target. The distortion may occur in the phase and amplitude information of a target. The parameter which obstructs this comparability of measurements from different polarisation channels is known as *channel imbalance*. It represents both amplitude imbalance and phase imbalance (Abhisek, Shashi and Valentyn 2019). To reduce the undesirable attenuation by a polarized channel on the measurements of the other polarized channels, isolation of the polarization channels is required. *Cross talk* is defined as distortions in the polarimetric data due to improper channel isolation.

Polarimetric calibration of radar data assumes backscatter symmetry and is based on statistical comparison of the data with ideal theoretical models. A typical point target occupies more than one pixel due to smaller pixel spacing in the SAR image compared to spatial resolution, which leads to error in estimation of Radar Cross Section (RCS). Radiometric calibration of the polarimetric data minimizes the error in the RCS estimation. To ensure the cross-pol reciprocity and to minimize the error due to imperfect isolation of polarimetric channels, calibration techniques for minimisation of crosstalk and channel imbalance are adopted.

## **Airborne SAR:**

SAR data can be acquired by using manned aerial vehicles or unmanned aerial vehicles. The recent L-band airborne campaigns by ISRO (L&S airborne SAR) and JPL, NASA are UAVSAR, (Alexander, Bruce and Brian 2014). These aerial vehicles carry polarimetric radar system which operates at a particular frequency, and are capable to acquire repeat tracks of SAR data. UAVSAR is an Uninhabited Aerial Vehicle Synthetic Aperture Radar operates at 1.25 GHz frequency which gives fully polarimetric SAR data. UAVSAR carry the radar instrument which is in a pod mounted to the fuselage of a Gulfstream III jet as shown in **Figure 2**. The aircraft flies at an altitude of 12.5 km and maps a 20 km swath with incidence angles ranging from 25° to 65°. Fully polarimetric Single Look Complex (SLC) images are available with range and azimuth pixels spacing of 1.66 m and 1 m respectively.

ISRO's L&S airborne SAR is a pre-cursor to upcoming space-borne NASA-ISRO Synthetic Aperture Radar (NISAR) mission. Development of dual frequency L- and S-band synthetic aperture radar (NISAR) is under progress by ISRO in collaboration with Jet Propulsion Laboratory (JPL), NASA. The NASA-ISRO Dual frequency SweepSAR (NISAR) has been conceptualized to provide L and S band space-borne SAR data with high repeat cycle, high resolution, and larger swath, with capability of full-polarimetric and Interferometric modes of operation.

The space borne SAR system transmits the pulse through the ionised plasma of the ionosphere. The system is exposed to Faraday rotation, that effect the induced magnetic field of the ionosphere, rotates the polarization plane of the radar signal giving rise to non-reciprocity condition (Masanobu, et al. 2013). Aircraft cannot fly over the ionosphere due to engineering limitations. The flying height of airborne platform is less compared to height of space borne platform. The polarization plane of the airborne SAR signal is unaffected by Faraday rotation, as their signals never pass through a dense electromagnetic field like ionosphere. In this case, the effect of earth curvature on the antenna is negligible, which is safe to assume flat earth throughout a scene of an airborne radar image as shown in **Figure 1**.

Where,  $R$  = effective slant range of the point;  $h$  = aircraft flying height

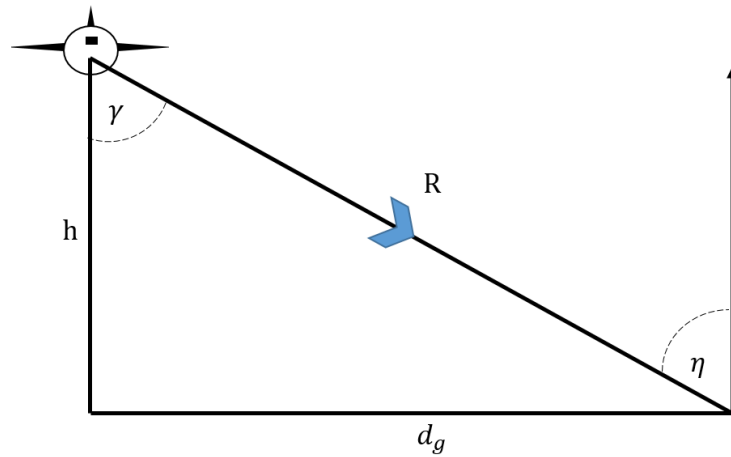


Figure 1. Local incidence angle ( $\eta$ ) and look angle ( $\gamma$ ) of airborne SAR assuming flat earth



Figure 2. UAVSAR/Gulfstream-III at an airport. UAVSAR Antenna is contained in the pod mounted under the GIII body

## 2 OBJECTIVES

The main objective of the study is to evaluate the radiometric and polarimetric calibration of L band quad polarized (HH, HV, VH, VV) data. Due to limited number of dataset available for ISRO's L&S airborne SAR mission, full-pol data acquired by UAVSAR campaigned by JPL NASA is used in this study to derive the polarimetric distortion matrix (PDM) and validate the results. Once validated, this will be used to carry out the polarimetric calibration of ISRO's L&S airborne SAR and NISAR full-pol data.

### 3 STUDY AREA

The study area is Rosamond dry lake placed between Antelope Valley and Mojave Desert in the southern of California, USA. It is naturally formed dry lake bed with a large flat surface of 35km<sup>2</sup>. This site is best suited for calibration purpose, because the study area is characterised by least amount of vegetation and the surface has curvature variation of less than 40 cm shown in **Figure 3**.(Abhisek, Shashi and Valentyn 2019). At the dry lake, array of trihedral corner reflectors of different sizes has been deployed for calibration purpose. Corner reflectors of 2.4 m (**Figure 4**), 4.8 m, 0.7 m sizes are sensed by L band, P band and Ka band sensor respectively. For L band there are 10 CR with East facing (350 heading) and 13 CR with West facing -170 heading with respect to North(Ronald, Elaine and Alex Fore 2015)

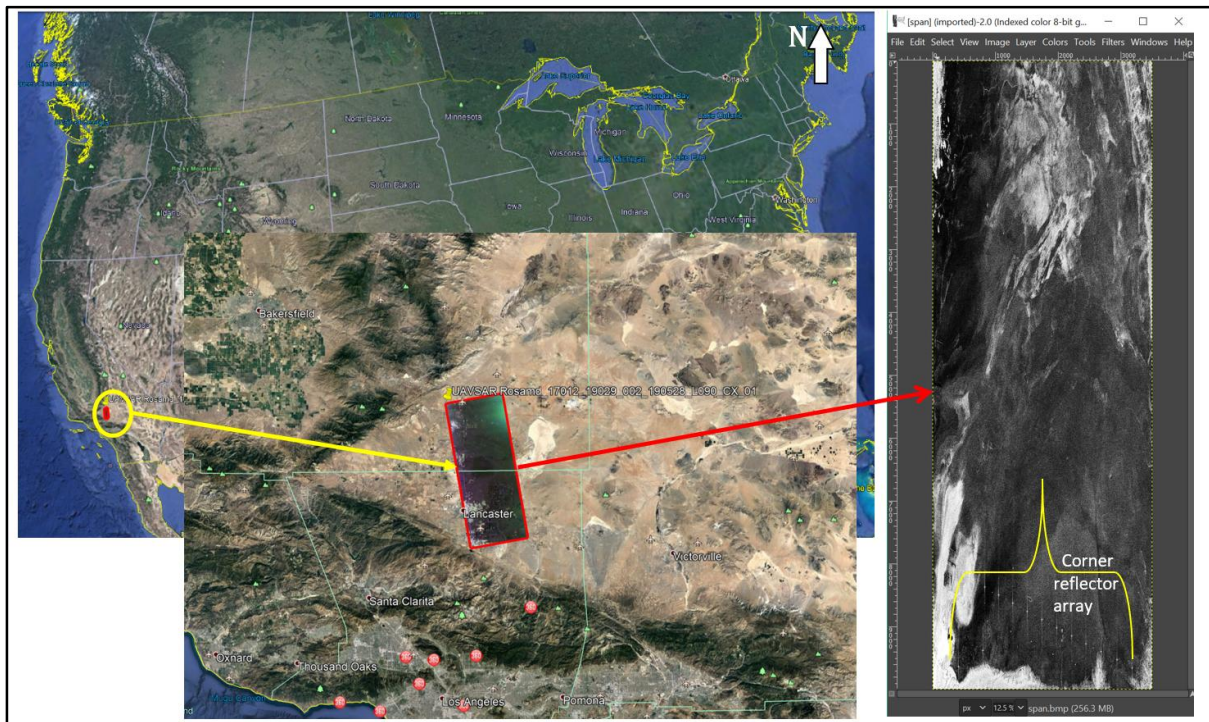


Figure 3. Google Earth image showing study area footprint (left image) and display of deployed corner reflectors at Rosamond dry lake bed (right image)

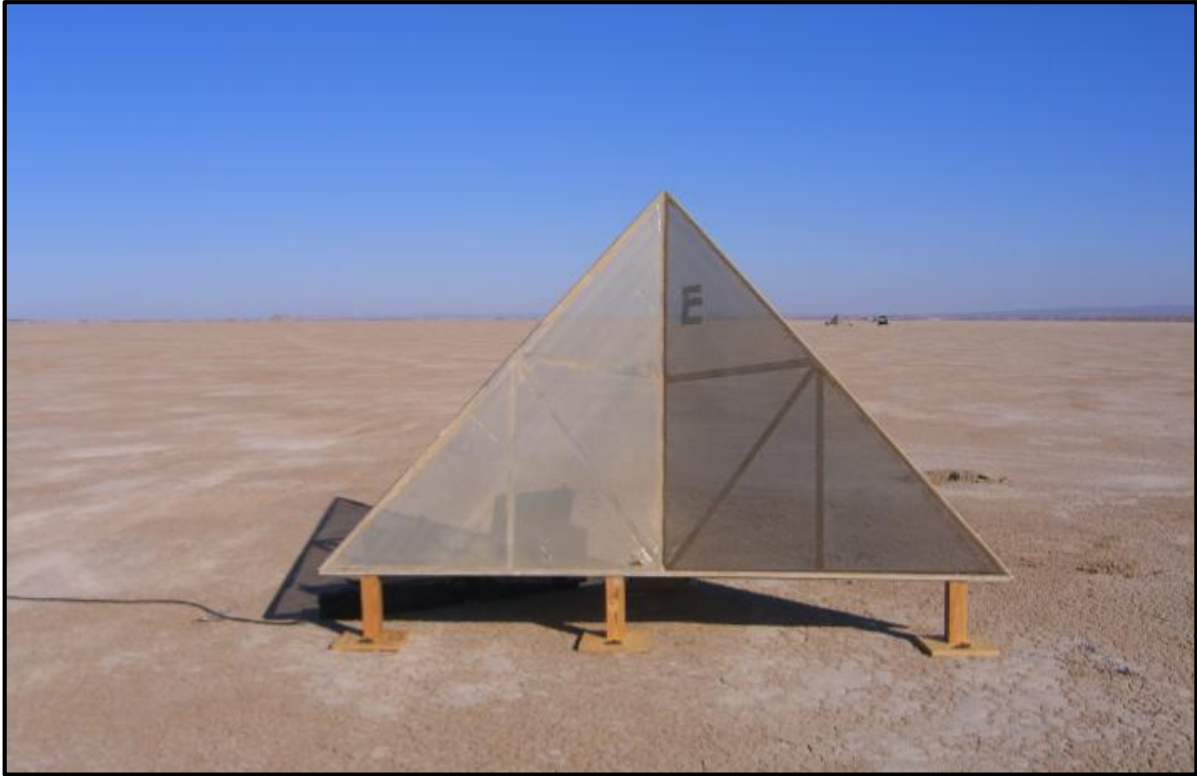


Figure 4. 2.4-meter trihedral triangular corner reflector

#### 4 **DATA USED**

Fully polarimetric radar data of single look complex slant range images of the study area are acquired from Jet Propulsion Laboratory (JPL) - website which is maintained by NASA. The following URL (<http://uavsar.jpl.nasa.gov/>) is used to download the following data, as shown in **Table 1** and **Table 2**. As shown in **Figure 5** there are 13 trihedral corner reflectors which are visible in the scene and are useful for this study.

Table 1. List of precision data files and radar parameters of SLC imagery

<b>Data type</b>	<b>Data files</b>	<b>Rows</b>	<b>Columns</b>
Data acquisition: 28 <sup>th</sup> May 2019			
SLC	Rosamd_17012_19029_002_190528_L090HH_CX_01.slc	92253	9900
	Rosamd_17012_19029_002_190528_L090HV_CX_01.slc		

	Rosamd_17012_19029_002_190528_L090VH_CX_01.slc		
	Rosamd_17012_19029_002_190528_L090VV_CX_01.slc		
<b>Site</b>	Rosamond, California, USA	<b>Data frequency</b>	1.2575 GHz (L band)
<b>Looking direction</b>	Left	<b>Acquisition mode</b>	Quad pol (HH, HV, VH, VV)
<b>Byte order</b>	Little Endian	<b>Complex type</b>	F-Complex
<b>Range Resolution</b>	1.8 meter	<b>Azimuth Resolution</b>	0.8 meter
<b>Bore sight</b>	90 degree		

**Software's:** Open source software such as PolSARpro V.6.0, ENVI Classic V.5.4 and GammaMsys-2 (licensed software) software's were used in this study.

Table 2. List of precision data files and radar parameters of Multilook imagery

<b>Data type</b>	<b>Data files</b>	<b>Rows</b>	<b>Columns</b>
Data acquisition: 28 <sup>th</sup> May 2019			
GRD	Rosamd_17012_19029_002_190528_L090HHHH_CX_01_ML 3X3.grd	3192	2083
	Rosamd_17012_19029_002_190528_L090HHHV_CX_01_ML 3X3.grd		
	Rosamd_17012_19029_002_190528_L090HHVV_CX_01_ML 3X3.grd		
	Rosamd_17012_19029_002_190528_L090HVHV_CX_01_ML 3X3.grd		
	Rosamd_17012_19029_002_190528_L090HVVV_CX_01_ML 3X3.grd		
	Rosamd_17012_19029_002_190528_L090VVVV_CX_01_ML 3X3.grd		
<b>Data frequency</b>	1.2575 GHz (L band)	<b>Acquisition mode</b>	Quad pol
<b>Byte order</b>	Little Endian	<b>Bore sight</b>	90 degree
<b>Range Resolution</b>	-0.000166680 degrees	<b>Azimuth Resolution</b>	0.000166680 degrees

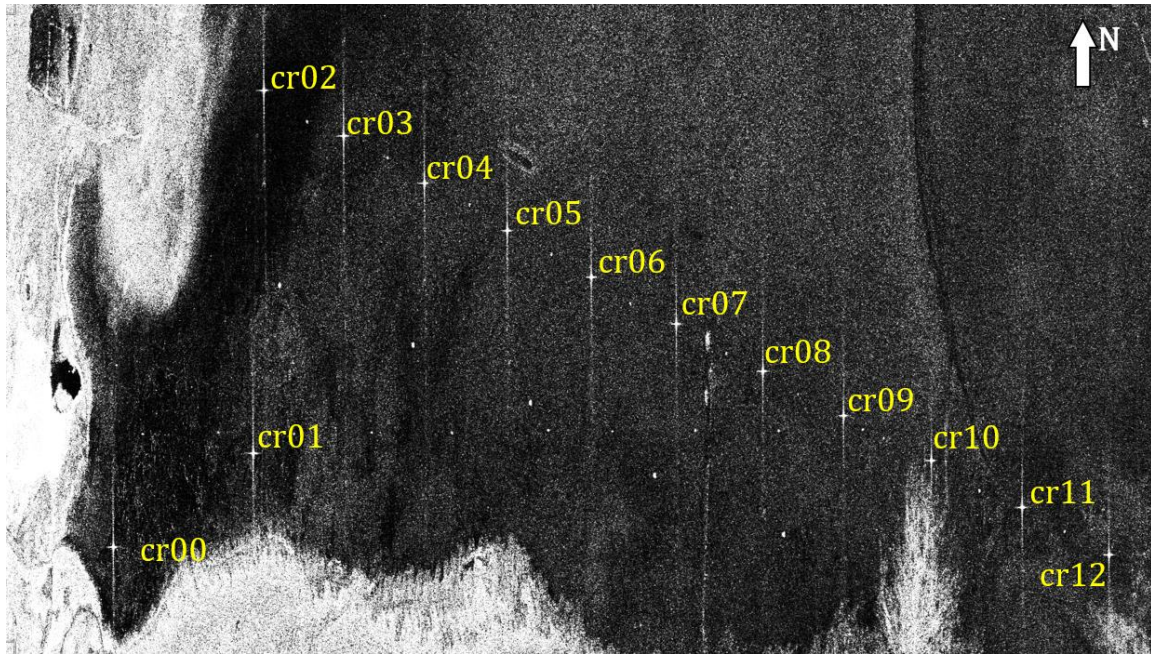


Figure 5. SLC image of HH-pol showing corner reflectors deployed at Rosamond dry lake

#### 4.1 POLARIMETRIC TARGET DESCRIPTIONS

Radar polarimetry is science of acquiring, processing and analysing the polarization state of an electromagnetic wave (Pottier, Lee and Famil 2007). The polarization information contained in the backscatter wave is highly related to the targets geometrical structure, orientation and geographical properties such as humidity, roughness and soil conductivity. This characteristic information can be completely described by scattering matrix  $S$  or coherent matrix  $T$  or covariance matrix  $C$ .

##### 4.1.1 Scattering Matrix (S)

SAR system is a high resolution radar capable of measuring the complex form of reflectivity of the target. A SAR image represents the scattering matrix element  $S_{pq}$  in complex form or radar cross section  $\sigma_{pq}$  in terms of intensity for the receive ( $q$ ) and transmit ( $p$ ) waves of the radar (Freeman 1995). The horizontal and vertical components helps to describe electromagnetic wave ( $E$ ) and given by Equation 1:

$$\begin{pmatrix} E_h^s \\ E_v^s \end{pmatrix} = \frac{e^{jk_0R}}{R} \begin{pmatrix} S_{hh} & S_{hv} \\ S_{vh} & S_{vv} \end{pmatrix} \begin{pmatrix} E_h^i \\ E_v^i \end{pmatrix}$$

**Equation 1. Components of Electromagnetic wave**

Where,

i = electric field vector of the incident wave.

s = electric field vector of the scattered wave.

$k_0$  = wavenumber of the illuminating wave.

R = radar distance between target and radar antenna.

The four elements of the scattering matrix are complex and these elements are measured from the magnitudes and phases measured by the four channels of a polarimetric radar (Polarimetric Analysis of Airborne DLR-ESAR for Vegetation Characterization 2012). These scattering properties vary with frequency and look angle of the radar. For linear polarization the scattering matrix (S) is measured using two polarized antennas and defined as in Equation 2 which is a 2x2 matrix:

$$[S] = \begin{bmatrix} S_{HH} & S_{HV} \\ S_{VH} & S_{VV} \end{bmatrix}$$

**Equation 2. Scattering matrix (S)**

The intensity in the cross polarization terms is much lesser than the co-pol terms, which is influenced by background and instrument noise. In case of mono-static configuration, scattering matrix is assumed symmetrical, reciprocity theorem  $S_{HV} = S_{VH}$  is applied, and has three independent elements in a full polarimetric system. In case of bi-static configuration, scattering matrix is not symmetric. Various polarimetric features can be derived from the scattering matrix or vector. The scattering matrix is transformed into scattering vector on Pauli basis and used for decomposition techniques and is given by Equation 3.

$$\text{Scattering vector, } V = \frac{1}{\sqrt{2}} \begin{bmatrix} S_{HH} + S_{VV} \\ S_{HH} - S_{VV} \\ 2S_{HV} \end{bmatrix}$$

**Equation 3. Scattering vector (V) derived from Pauli basis**

#### 4.1.2 Covariance (C) and Coherency (T) Matrices

The covariance and coherence matrices are derived from scattering matrix. It explains the relation between received signals in the channels of polarimetric radar and describes the scattering properties of the target. In mono static condition, reciprocity symmetry is assumed and 3x3 matrices were obtained such as Equation 6 and Equation 8. In case bi-static, symmetry cannot be assumed, and 4x4 matrices were obtained such as Equation 7 and Equation 9.

A covariance or coherence matrix is a second order statistics of scattering matrix elements and it is Hermitian semi definite positive matrix. These matrices are constructed from a unitary target vector obtained from the projection of a scattering matrix onto a reduced and modified Pauli spin matrix set.

##### Covariance Matrix

System vectors such as Equation 4 and Equation 5 are constructed from the backscattering matrix [S], that helps to extract information of the target. The matrix is based on lexicographic combinations of scattering matrix elements. The factor  $\sqrt{2}$  helps to keep the norm of the target vector invariant, which is equal to the total power scattered by the target. (Pottier, Lee and Famil 2007)

$$k_{3L} = [S_{11} \ S_{12}\sqrt{2} \ S_{22}]$$

Equation 4. Scattering vector for mono-static case

$$k_{4L} = [S_{11} \ S_{12}S_{21}S_{22}]$$

Equation 5. Scattering vector for bi-static case

$$[C_3] = k_{3L}k_{3L}^\dagger = \begin{bmatrix} |S_{hh}|^2 & \sqrt{2}S_{hh}S_{hh}^* & S_{hh}S_{vv}^* \\ \sqrt{2}S_{hv}S_{hv}^* & 2|S_{hv}|^2 & \sqrt{2}S_{hv}S_{vv}^* \\ S_{vv}S_{hh}^* & \sqrt{2}S_{vv}S_{hv}^* & |S_{vv}|^2 \end{bmatrix}$$

Equation 6. Covariance 3x3 matrix for mono-static case

Where \* represents the conjugate and † represents the conjugate transpose.

$$[C_4] = k_{4L}k_{4L}^\dagger = \begin{bmatrix} \langle |S_{HH}|^2 \rangle & \langle S_{HH}S_{HV}^* \rangle & \langle S_{HH}S_{VH}^* \rangle & \langle S_{HH}S_{VV}^* \rangle \\ \langle S_{HV}S_{HH}^* \rangle & \langle |S_{HV}|^2 \rangle & \langle S_{HV}S_{VH}^* \rangle & \langle S_{HV}S_{VV}^* \rangle \\ \langle S_{VH}S_{HH}^* \rangle & \langle S_{VH}S_{HV}^* \rangle & \langle |S_{VH}|^2 \rangle & \langle S_{VH}S_{VV}^* \rangle \\ \langle S_{VV}S_{HH}^* \rangle & \langle S_{VV}S_{HV}^* \rangle & \langle S_{VV}S_{VH}^* \rangle & \langle |S_{VV}|^2 \rangle \end{bmatrix}$$

Equation 7. Covariance 4x4 matrix for bi-static case

## Coherency Matrix

Coherency matrix is obtained from scattering matrix in Pauli basis form and same as the covariance matrix.

$$[T_3] = k_{3L} k_{3L}^\dagger = \frac{1}{2} \begin{bmatrix} \langle |S_{HH} + S_{VV}|^2 \rangle & \langle (S_{HH} + S_{VV})(S_{HH} - S_{VV})^* \rangle & 2 \langle (S_{HH} + S_{VV})S_{HV}^* \rangle \\ \langle (S_{HH} - S_{VV})(S_{HH} + S_{VV})^* \rangle & \langle |S_{HH} - S_{VV}|^2 \rangle & 2 \langle (S_{HH} - S_{VV})S_{HV}^* \rangle \\ 2 \langle S_{HV}(S_{HH} + S_{VV})^* \rangle & 2 \langle S_{HV}(S_{HH} - S_{VV})^* \rangle & 4 \langle |S_{HV}|^2 \rangle \end{bmatrix}$$

**Equation 8. Coherency 3x3 matrix for mono-static case**

$$[T_4] = k_{4L} k_{4L}^\dagger = \begin{bmatrix} T_{11} & T_{12} & T_{13} & T_{14} \\ T_{12}^* & T_{22} & T_{23} & T_{24} \\ T_{13}^* & T_{23}^* & T_{33} & T_{34} \\ T_{14}^* & T_{24}^* & T_{34}^* & T_{44} \end{bmatrix}$$

**Equation 9. Coherency 4x4 matrix for bi-static case**

The Eigen values of the above matrices are positive, real semi definite Hermitian (Pottier, Lee and Famil 2007). Span of the data is defined as the sum of the diagonal elements is proportional to the total received power from the polarimetric channels. The first diagonal elements of the matrices give the single bounce scattering information, the second diagonal elements give double bounce scattering information and third diagonal elements gives information about volume scattering.

## 5 METHODOLOGY

The below mentioned methodology is followed to achieve the objectives in this work.

Primarily the un-calibrated full pol dataset is used to obtain the parameters mentioned in the steps below.

- Absolute calibration constant (A) was estimated using the methodology given in (Alexander, Bruce and Brian 2014) and (Shweta, et al. 2017).
- Co-pol channel imbalance ( $f_i$ ) parameter and co-pol channel phase difference  $\phi_t + \phi_r$  are estimated at each corner reflector. Cross-pol channel imbalance (g) and cross-pol channel phase difference  $\phi_t - \phi_r$  are derived from a sufficiently large homogenous featureless patch (distributed target) of the scene.
- Estimated values of A,  $f_i$ , g,  $\phi_t + \phi_r$  and  $\phi_t - \phi_r$  are used in the correction of the dataset to obtain radiometric and phase calibrated dataset. Since phase difference between polarized channels (HH and VV) is  $1.5^\circ$  and less than the specified value of  $5^\circ$ , it is assumed that the dataset is well radiometrically and phase calibrated.
- Polarimetric signatures are generated using the above corrected dataset, and these signatures should match the ideal signature of corner reflector.
- Cross talks (u, v, w, z) and channel imbalance ( $\alpha$ , k) are estimated using the radiometric and phase corrected dataset. Quegan's algorithm (Quegan 1994) and Ainsworth algorithm (Ainsworth and Ferro-Famil 2006) are best calibration techniques which can be used to minimize the cross talks and channel imbalance. In this study, Quegan's algorithm was used to generate polarimetric distortion matrix (PDM).
- The above estimated u, v, w, z,  $\alpha$  and k values are then used in the cross talk and channel imbalance correction, generating polarimetric calibrated dataset.
- Polarimetric signatures are generated using the above corrected dataset and should match the ideal signature of corner reflector.

### 5.1 Radiometric and Phase Calibration

While applying the radiometric correction, two types of error occurs (a) SAR cross track antenna pattern error due to wrong measurement in the elevation angle between the radar and pixel location and (b) error in the slant range to ground range project of the pixel area due to misreading in the local incidence angle of that particular pixel (Freeman 1995). The

correction for the above two errors are applied to the dataset and are distributed by the JPL/NASA. Radiometric correction is to convert image pixel values into normalized radar cross section ( $\sigma_{cr}$ ) from Equation 13, which is an important goal in calibrating SAR images and estimated in section 6.1.1. Phase calibration is to minimize the phase bias present in both co-pol and cross-pol channels. Neglecting the cross talks and channel imbalances, radiometric and phase calibration is applied to the datasets as per Equation 10

$$S' = A \begin{bmatrix} s_{vv}f^2 e^{i(\phi_{t,v}+\phi_{r,v})} & s_{vh}\left(\frac{f}{g}\right)e^{i(\phi_{t,h}+\phi_{r,v})} \\ s_{hv}fge^{i(\phi_{t,v}+\phi_{r,h})} & s_{hh}e^{i(\phi_{t,h}+\phi_{r,h})} \end{bmatrix}$$

**Equation 10. Radiometric and Phase calibration model**

Where,  $S'$  = radiometric and phase calibrated scattering matrix from transmitted polarization 't' and received polarization 'r'.

$S_{vv}, S_{hh}, S_{vh}, S_{hv}$  = observed scattering matrix

$A$  = absolute calibration factor

$f$  = co-pol channel imbalance parameter

$g$  = cross-pol channel imbalance parameter

$\phi_{x,j}$  = phase error in-current when transmitting or receiving polarization 'j'

After removal of the arbitrary phase, Equation 10 reduces to Equation 11

$$S' = A \begin{bmatrix} s_{vv}f^2 e^{i(\phi_t+\phi_r)} & s_{vh}\left(\frac{f}{g}\right)e^{i(\phi_r)} \\ s_{hv}fge^{i(\phi_t)} & s_{hh} \end{bmatrix}$$

**Equation 11. Calibration model after removal of arbitrary phase**

Where,  $\phi_t = \phi_{t,v} - \phi_{t,h}$ ;  $\phi_r = \phi_{r,v} - \phi_{r,h}$

### **5.1.1 Estimation of Absolute Calibration Parameter (A):**

Absolute calibration parameter (A) is the calibration factor relating the SAR image intensity and radar cross section of the target (Masanobu, et al. 2013). It is obtained using

Equation 12 (Alexander, Bruce and Brian 2014) and Equation 13 (Ronald, Elaine and Alex Fore 2015).

$$10\log_{10} \left[ \frac{\sigma_{cr}}{(s_{hh}s_{hh}^*)} \right] = -10\log_{10}(A^2)$$

Equation 12. Estimation of absolute calibration parameter

$$\sigma_{cr} = 4\pi L^4 / \lambda^2 [\Omega(\theta_{cr}, \phi_{cr}) - 2/\Omega(\theta_{cr}, \phi_{cr})]^2$$

Equation 13. Estimation of RCS for triangular trihedral corner reflector

Where,  $\sigma_{cr}$  = RCS of a triangular trihedral corner reflector

$$\Omega(\theta_{cr}, \phi_{cr}) = \cos\theta_{cr} + (\sin\phi_{cr} + \cos\phi_{cr}) \sin\theta_{cr}$$

$\theta_{cr}$ : Incidence angle relative to the triangular trihedral corner reflector

$\phi_{cr}$ : Azimuth angle relative to one of the vertical side of the corner reflector (max. response of the corner reflector is at 45 deg.)

$\lambda$ : Wavelength of the radar signal

L = length of inner side of the triangular corner reflector (2.4384 meters)

### 5.1.2 Estimation of co-pol channel imbalance (f) and phase difference phi t

Co-pol channel imbalance parameters f and  $\phi_t + \phi_r$  are estimated using Equation 14 for each corner reflectors and mean value of them is considered as effective value. Phase anomaly  $\phi_t + \phi_r$  between HH and VV polarizations are estimated using Equation 15.

$$f = \left[ \frac{s_{vv}s_{vv}^*}{s_{hh}s_{hh}^*} \right]^{1/4}$$

Equation 14. Estimation of parameter f

$$\phi_s = \arg(s_{vv}s_{hh}^*)$$

Equation 15. Phase difference between HH and VV pol channels

Where,  $\phi_s = \phi_t + \phi_r$

### 5.1.3 Estimation of cross-pol channel imbalance (g) and phase difference phi r

Cross-pol channel imbalance parameters  $g$  and  $\phi_t - \phi_r$  are estimated using homogenous distributed target of 700x 700 pixels from the image as per Equation 16. Phase anomaly  $\phi_t - \phi_r$  between HV and VH polarizations are estimated using Equation 17.

$$g = \left[ \frac{\langle s_{hv} s_{hv}^* \rangle}{\langle s_{vh} s_{vh}^* \rangle} \right]^{1/4}$$

Equation 16. Estimation of parameter g

$$\phi_d = \arg(s_{hv} s_{vh}^*)$$

Equation 17. Phase difference between HV and VH pol channels

Where,  $\phi_d = \phi_t - \phi_r$

Phase anomaly at transmission  $\phi_t$  and reception  $\phi_r$  is estimated using Equation 15 and Equation 17

$$\phi_t = \frac{\phi_s + \phi_d}{2}$$

$$\phi_r = \frac{\phi_s - \phi_d}{2}$$

## 5.2 Polarimetric Calibration

Polarimetric SAR data calibration is an important process to ensure accurate extraction of the geophysical properties of the target. Calibration is required to understand polarimetric signatures of the target and also to compare observations between scenes and theory (Quegan 1994). To transform data into quantitative parameter such as biophysical or geophysical properties, it is necessary to assure that dataset is not contaminated. The distortion matrices which is estimated express the polarimetric transformation between transmission and reception using channel imbalance and cross talks (Chen, Tao and Xueliang 2011). In Airborne SAR system, the cross talk is range dependent and cannot be neglected which becomes an important step for polarimetric calibration procedure.

Well established Quegan and Ainsworth cross talk correction models are available and detailed description of these models are defined in the following sections.

### 5.2.1 Distortion Models

#### Quegan's Algorithm

The calibration algorithm proposed by Quegan is more general approach and is today standards for cross talk calibration of the polarimetric data. This unified approach has been applied to the scattering matrix and it relies on the scene dominated by the targets. The algorithm requires unsymmetrical data and uses quantities derived from the covariance matrix. It permits ready interpretation of the terms in the calibration procedure without system reciprocity assumption. The following are the assumptions are used to perform cross talk calibration. The acquired dataset is fully polarimetric and available in the form of the scattering matrix.

- 1) The observed scattering matrix can be modeled as a linear system.
- 2) Scattering reciprocity is satisfied unless the target is physically altered  $S_{ij} = S_{ji}$ .
- 3) In case of distributed targets, cross polarized channels are not correlated  $\langle S_{ij}S_{ij}^* \rangle = 0$ .
- 4) The off diagonal terms of the matrices [R] and [T] are small compared to the diagonal terms.

The systems effects are modeled by two stage linear process so that observed data matrix  $S'$  can be written as

$$S' = RST + N$$

Where, R and T are phase and amplitude distortions introduce on receive and transmit and N is system noise. The above expression can be rewritten as

$$[S'] = [M][S] + [N]$$

Where,

$$[S'] = \text{observed scattering matrix in the form of } (S'_{HH}, S'_{HV}, S'_{VH}, S'_{VV})^T$$

$$[S] = \text{True scattering matrix in the form of } (S_{HH}, S_{VH}, S_{VV})^T$$

$$[M] = \text{Distortion matrix of dimension } (4 \times 3)$$

$$[N] = \text{System noise matrix } (N_{HH}, N_{HV}, N_{VH}, N_{VV})^T$$

Due to condition (3) and (4), the region being calibrated is dominated by targets for, which the vector S of the covariance matrix  $\langle C_s \rangle$  gets reduced to (1)

$$\langle C_s \rangle = \begin{bmatrix} \sigma_{HH} & 0 & \rho \\ 0 & \sigma_{VH} & 0 \\ \rho^* & 0 & \sigma_{VV} \end{bmatrix} \text{-----(1)}$$

Where,

$$\sigma_{ij} = \langle S_{ij} S_{ij}^* \rangle; \quad \rho = \langle S_{HH} S_{VV}^* \rangle = \langle S_{VV} S_{HH}^* \rangle^*$$

Now, observed covariance matrix (C) of [S'] is given by (2) ignoring system noise

$$C = M C_s M^\dagger \text{-----(2)}$$

Where M<sup>†</sup> is the conjugate transpose of M

Distortion matrix can be expressed as

$$M = Y \begin{pmatrix} \alpha & v + \alpha w & vw \\ \alpha u & \alpha & v \\ \alpha z & 1 & w \\ \alpha uz & u + \alpha z & 1 \end{pmatrix} \begin{pmatrix} k^2 & 0 & 0 \\ 0 & k & 0 \\ 0 & 0 & 1 \end{pmatrix} \text{ eqn - (3)}$$

This distortion matrix consists six unknowns u,v,w,z are the complex crosstalk parameters and  $\alpha$ , k are the complex channel imbalance parameters. u, v, w, z can be obtained from eqn - (4)

$$\begin{aligned} u &= (C_{44} C_{21} - C_{41} C_{24}) / \Delta \\ v &= (C_{11} C_{24} - C_{21} C_{14}) / \Delta \\ z &= (C_{44} C_{31} - C_{41} C_{34}) / \Delta \\ w &= (C_{11} C_{34} - C_{31} C_{14}) / \Delta \\ \Delta &= C_{11} C_{44} - |C_{14}|^2 \end{aligned} \quad \left. \vphantom{\begin{aligned} u \\ v \\ z \\ w \\ \Delta \end{aligned}} \right\} \text{ eqn - (4)}$$

The term  $\alpha$  can be derived as shown in equation (5), assuming the random noises in cross polarized channels are equal, i.e.  $N_{VH} = N_{HV}$

$$\begin{aligned} \alpha &= \frac{|\alpha_1 \alpha_2| - 1 + \sqrt{(|\alpha_1 \alpha_2| - 1)^2 + 4|\alpha_2|^2}}{2|\alpha_2|} \frac{\alpha_1}{|\alpha_1|} \\ \alpha_1 &= \frac{C_{22} - u C_{12} - v C_{42}}{X} \\ \alpha_2 &= \frac{X^*}{C_{33} - z^* C_{31} - w^* C_{34}} \\ X &= C_{32} - z C_{12} - w C_{42} \\ k &= \frac{1}{\sqrt{a}} \end{aligned} \quad \left. \vphantom{\begin{aligned} \alpha \\ \alpha_1 \\ \alpha_2 \\ X \\ k \end{aligned}} \right\} \text{ eqn - (5)}$$

### 5.2.2 Polarimetric signatures

Polarization signature is defined as a plot of the backscattered power received from the target (corner reflector) as a function of the polarization of the incident wave and backscattered electromagnetic wave. It helps in visualization and analysis of backscatter behaviour of a target (Polarimetric Analysis of Airborne DLR-ESAR for Vegetation Characterization 2012). The polarization of a wave is described by four independent variables: - (a) the ellipticity of the incident wave; (b) the orientation of the incident wave (c) the ellipticity of the backscattered wave and (d) the orientation of the backscattered wave. Only two variables either ellipticity and orientation of the incident wave/ backscattered wave are used at a time to portray the co-pol and cross-pol signatures.

In co-pol case, the polarization of the scattered wave is same as polarization of the incident wave, while for the case of cross-polarization, the polarization of the scattered wave is orthogonal to the polarization of the incident wave. Co-polarization signature of “ridge shape” and Cross-polarization signature of “valley shape” are generated due to change in ellipticity sign of the polarimetric data. For linear polarization, the co-pol response is unity and cross-pol response is zero. These signatures help in identifying different surface scatterer.

The polarimetric signature can be generated using electromagnetic wave synthesis. The synthesised scattering matrix ( $[S_{syn}]$ ) can be generated from the actual scattering matrix ( $[S]$ ) with respect to varying ellipticity angle ( $\chi$ ) and orientation angle ( $\psi$ ).

$$S_{syn} = [R_{\psi}][S][R_{\chi}]$$

Where,

$$[R_{\psi}] = \begin{bmatrix} \cos\psi & -\sin\psi \\ \sin\psi & \cos\psi \end{bmatrix}; [R_{\chi}] = \begin{bmatrix} \cos\chi & -j \sin\chi \\ -j \sin\chi & \cos\chi \end{bmatrix}$$

## 6 RESULTS AND DISCUSSIONS

### 6.1 Radiometric and Phase Parameters

The inputs used to estimate the Radar Cross Section (RCS) of each corner reflector are shown in Table 3. The difference between theoretical RCS and estimated RCS for HH and VV polarization is estimated using GAMMA –Msys 2 software. GAMMA software estimates the RCS, by using integral power method(Shweta, et al. 2017).

Table 4 gives the pixel values of number of clutters locations considered in the process of RCS estimation and deviation from theoretical RCS. The RCS difference of each CR is found to be less than 1dB for both the polarization channels as shown in Figure 6, which shows that the dataset is radiometrically corrected. Impulse Response function of each corner reflector (Figure 10) is generated for HH polarizations as shown in Figure 11 and VV polarizations as shown in Figure 12 respectively. The average peak power value of each CR and the difference between peak powers of HH and VV channels are illustrated in Figure 7 and Figure 8 respectively.

Table 3. Attributes used to calculate RCS of each CR with respect to Incidence and Azimuth angle

Corner reflector ID	Elevation angle + incidence angle @CR (deg)	incidence angle (in radians)	$\Omega = \cos(\theta) + (\sin\phi + \cos\phi)\sin(\theta)$	$4*\pi*a*a*a*a*\lambda*\lambda$	Square $(\Omega-2/\Omega)$	RCS
0	53.4286	0.9325	1.7316	7816.58	0.332467	2598.752
1	57.11211	0.9968	1.730561	7816.58	0.330472	2583.158
2	56.88715	0.9929	1.73083	7816.58	0.330987	2587.186
3	57.93546	1.0112	1.72935	7816.58	0.328153	2565.037
4	58.14773	1.0149	1.72898	7816.58	0.327446	2559.51
5	58.36418	1.0186	1.728579	7816.58	0.326679	2553.514
6	60.01325	1.0474	1.724708	7816.58	0.319328	2496.056
7	62.91842	1.0981	1.714417	7816.58	0.300128	2345.974
8	60.67854	1.0590	1.722742	7816.58	0.315621	2467.08
9	62.44762	1.0899	1.716385	7816.58	0.30376	2374.367
10	61.16324	1.0675	1.721163	7816.58	0.312658	2443.917

<b>11</b>	62.92029	1.0982	1.714409	7816.58	0.300113	2345.858
<b>12</b>	63.11911	1.1016	1.713543	7816.58	0.29852	2333.409

**Azimuth angle in radians ( $\varphi$ ) = 0.785398163 (45 deg.)**

Table 4. Details of clutter and deviation of RCS from theoretical value

<b>CR</b>	<b>Clutter</b>	<b>Polarization</b>	<b>Theoretical RCS in m<sup>2</sup></b>	<b>Deviation of RCS from theoretical (in dB)</b>
<b>CR00 (2412,49637)</b>	C1 (2452, 49683)	HH VV	2598.752	-1.0138 -1.0135
<b>CR01 (2801,49376)</b>	C1	HH VV	2583.158	-0.8127 -0.6759
<b>CR02 (2831,48368)</b>	C2 (4132, 48936)	HH VV	2587.186	-0.9197 -0.6197
<b>CR03 (3053,48494)</b>	C2	HH VV	2565.037	-0.4903 -1.1652
<b>CR04 (3277,48626)</b>	C2	HH VV	2559.51	-0.0193 -0.1678
<b>CR05 (3508,48758)</b>	C2	HH VV	2553.514	-0.6766 -0.1305
<b>CR06 (3741,48887)</b>	C2	HH VV	2496.056	-0.7555 0.0883
<b>CR07 (3978,49017)</b>	C2	HH VV	2345.974	-0.3238 0.4119
<b>CR08 (4218,49148)</b>	C2	HH VV	2467.08	-0.4423 0.0916
<b>CR09 (4443,49272)</b>	C2	HH VV	2374.367	0.5184 0.7810
<b>CR10 (4687,49396)</b>	C3 (4623, 49458)	HH VV	2443.917	0.6300 0.4032
<b>CR11 (4939,49526)</b>	C4 (5050, 49583)	HH VV	2345.858	-0.1654 -0.1964
<b>CR12 (5181,49658)</b>	C4	HH VV	2333.409	0.2111 -0.2595
			<b><i>RCS diff. Mean in HH, VV (A)</i></b>	<b><i>0.9339 0.9574</i></b>

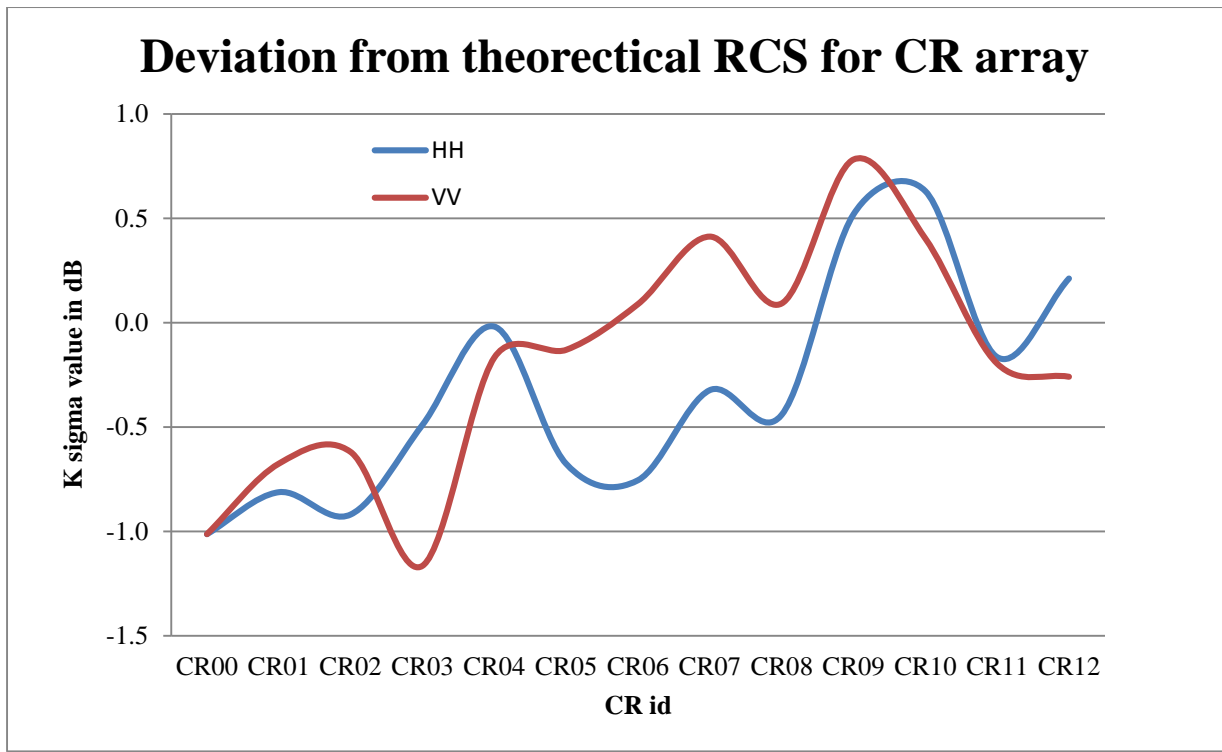


Figure 6. Graph showing RCS difference for HH and VV pol.

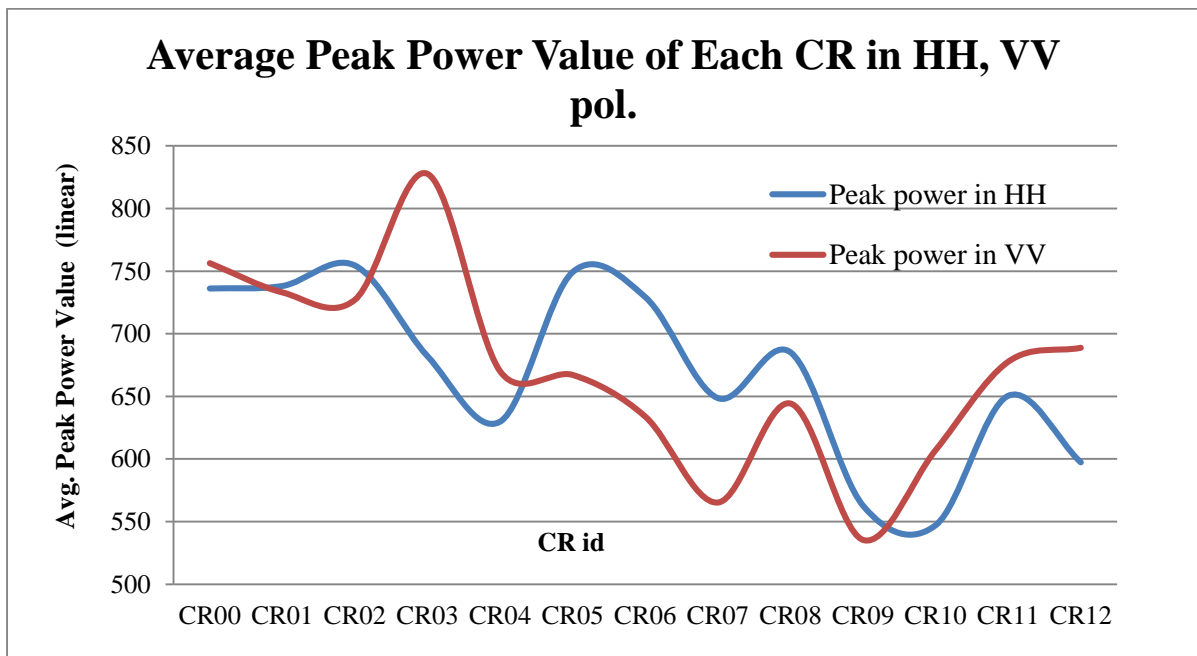


Figure 7. Graph showing peak power values for HH and VV pol. in linear amplitude units

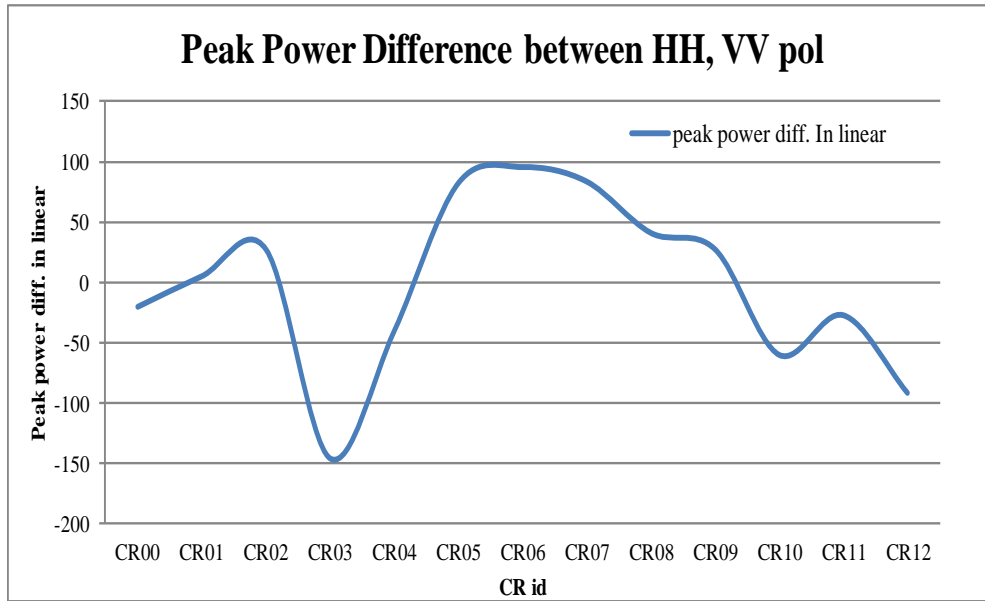


Figure 8. Graph showing peak power difference between HH and VV pol. in linear amplitude units

Peak phase values of each CR are calculated for HH and VV polarized channels as per Table 5. The peak phase difference of each CR for HH and VV channels are shown in Figure 9.

Table 5. Peak phase values for HH and VV polarization

CR	Peak Phase in HH pol. (in degrees)	Peak Phase in VV pol. (in degrees)	Peak Phase difference (VV- HH)
CR00	-121.487	-119.205	2.282
CR01	-130.337	-123.324	7.013
CR02	-238.713	-233.924	4.789
CR03	-68.943	-66.111	2.832
CR04	-66.739	-62.981	3.758
CR05	-69.134	-67.018	2.116
CR06	-319.303	38.106	357.409
CR07	-4.406	-2.057	2.349
CR08	-127.512	-131.084	-3.572
CR09	-182.427	-185.639	-3.212
CR10	-97.39	-98.558	-1.168
CR11	-244.346	-245.052	-0.706
CR12	-245.556	-243.097	2.459
		<b>Mean Phase in deg.(phi_s)</b>	<b>1.5783°</b>

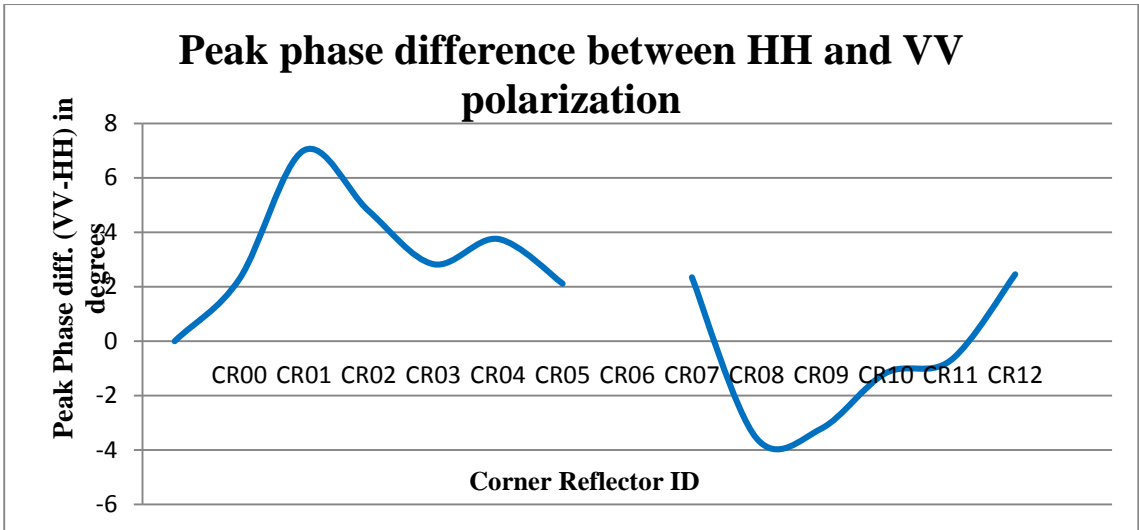


Figure 9. Graph showing phase difference HH-VV pol

Table 5. Range and Azimuth resolution estimated from IRF of the point targets

CR	Range_3dB width		Azimuth_3dB width	
	Estimated range resolution	Difference between estimated and specified range resolution (1.8 meter)	Estimated azimuth resolution	Difference between estimated and specified azimuth resolution (0.8 meter)
CR00	2.686	0.886	0.942	0.142
CR01	2.627	0.827	0.94	0.14
CR02	2.696	0.896	0.893	0.093
CR03	2.626	0.826	0.945	0.145
CR04	2.642	0.842	0.947	0.147
CR05	2.688	0.888	0.883	0.083
CR06	2.744	0.944	0.926	0.126
CR07	2.666	0.866	0.951	0.151
CR08	2.755	0.955	0.934	0.134
CR09	2.64	0.84	0.926	0.126
CR10	2.662	0.862	0.949	0.149
CR11	2.743	0.943	0.915	0.115
CR12	2.81	1.01	0.944	0.144

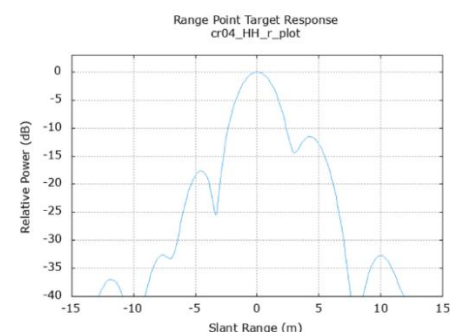
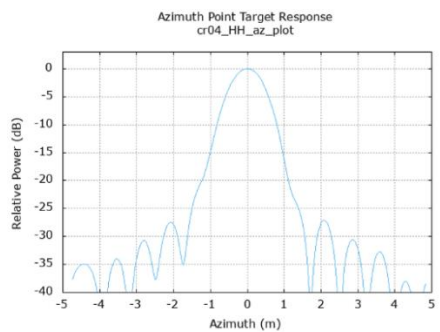
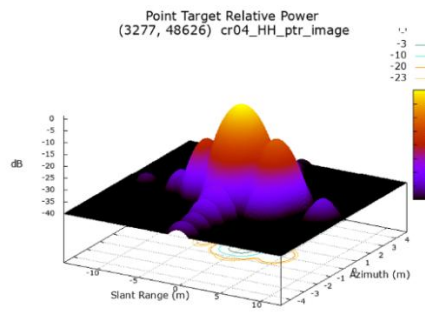
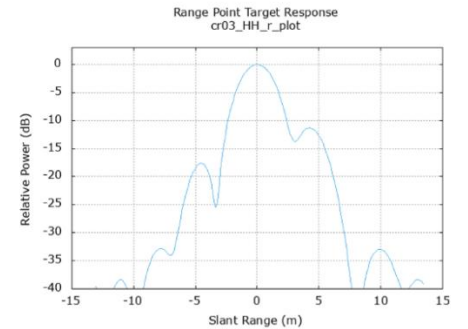
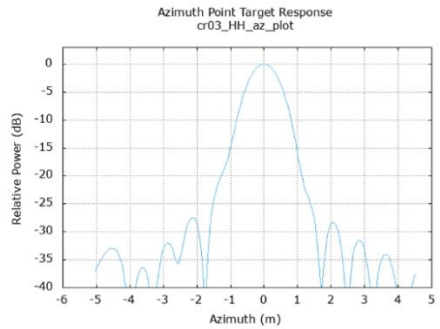
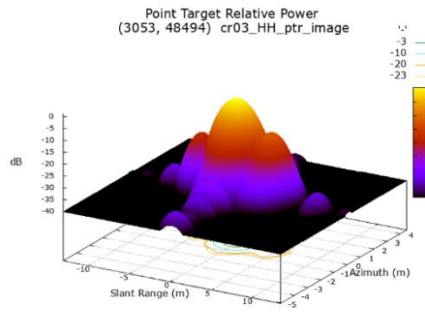
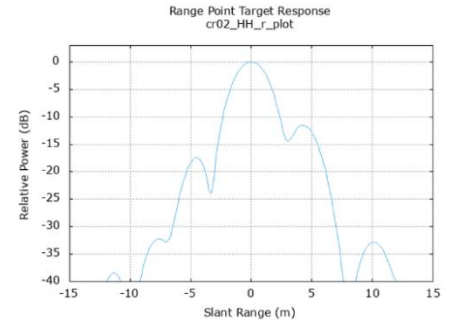
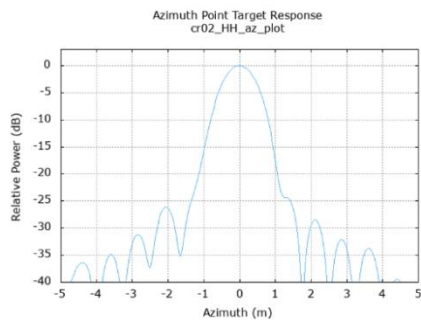
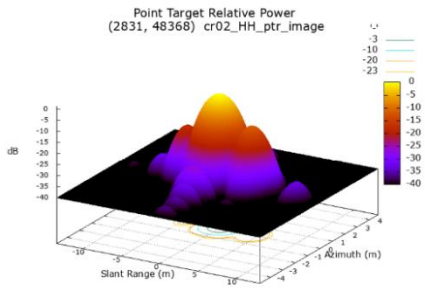
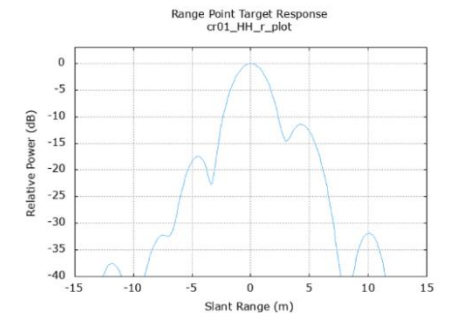
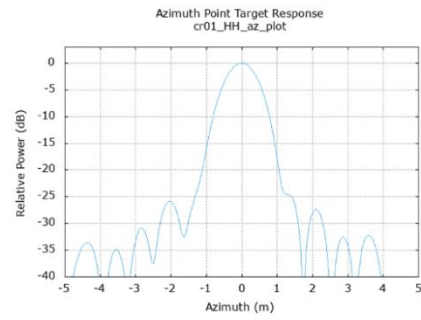
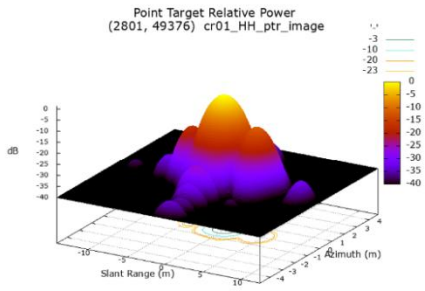
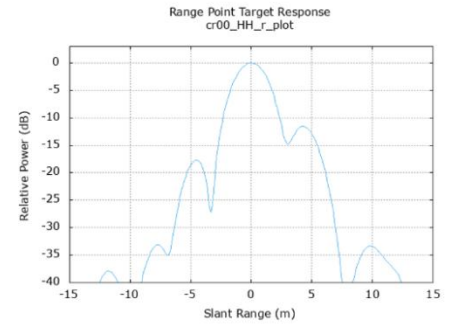
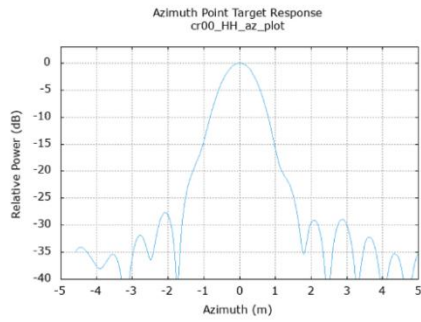
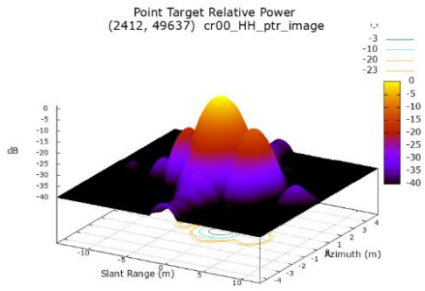
The range and azimuth resolution are estimated from the impulse response function of each corner reflector and their difference from the specified value is calculated and are shown in

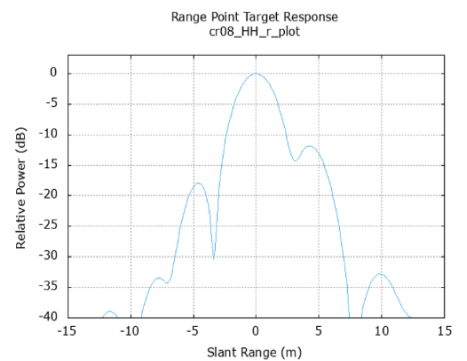
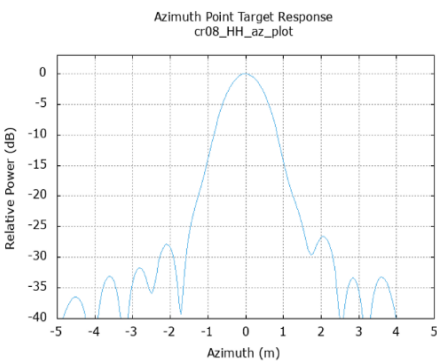
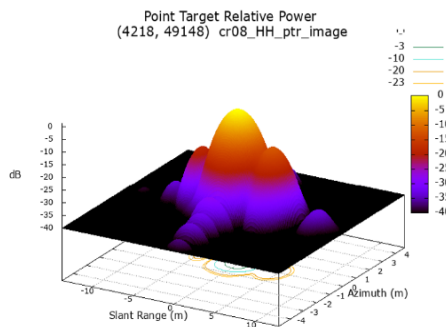
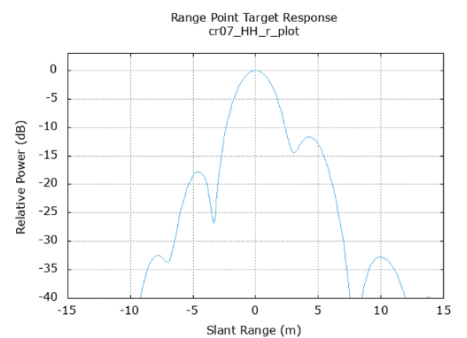
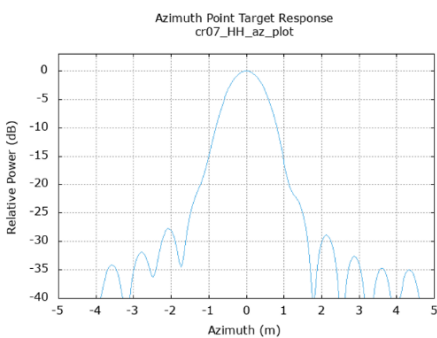
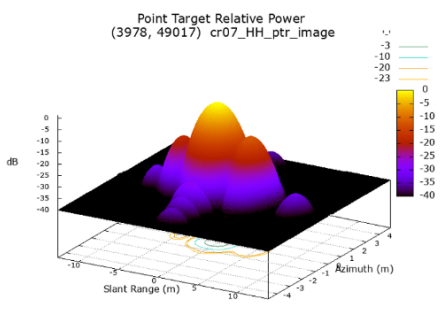
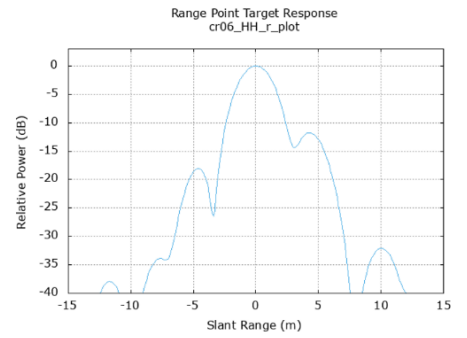
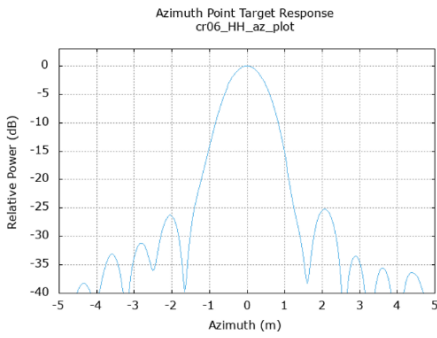
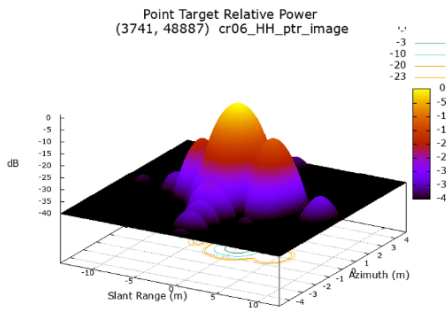
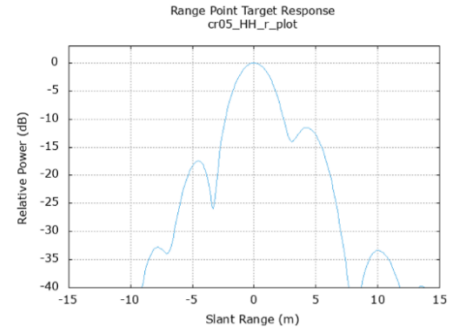
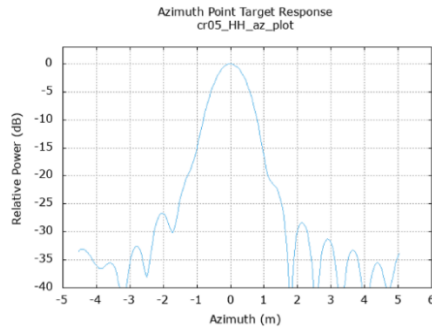
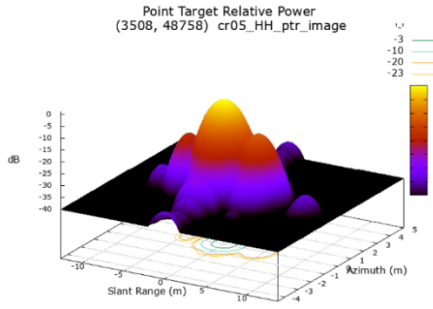
**Table 5.** The range resolution is found to be  $2.69 \pm 0.06$  meters and azimuth resolution as  $0.93 \pm 0.02$  meters and the difference from the specified value was found to be  $0.89 \pm 0.06$  and  $0.93 \pm 0.02$  for range and azimuth respectively.

### ***6.1.1 Impulse Response Functions for HH polarization***



Figure 10. Location of CR's in SLC image of HH pol





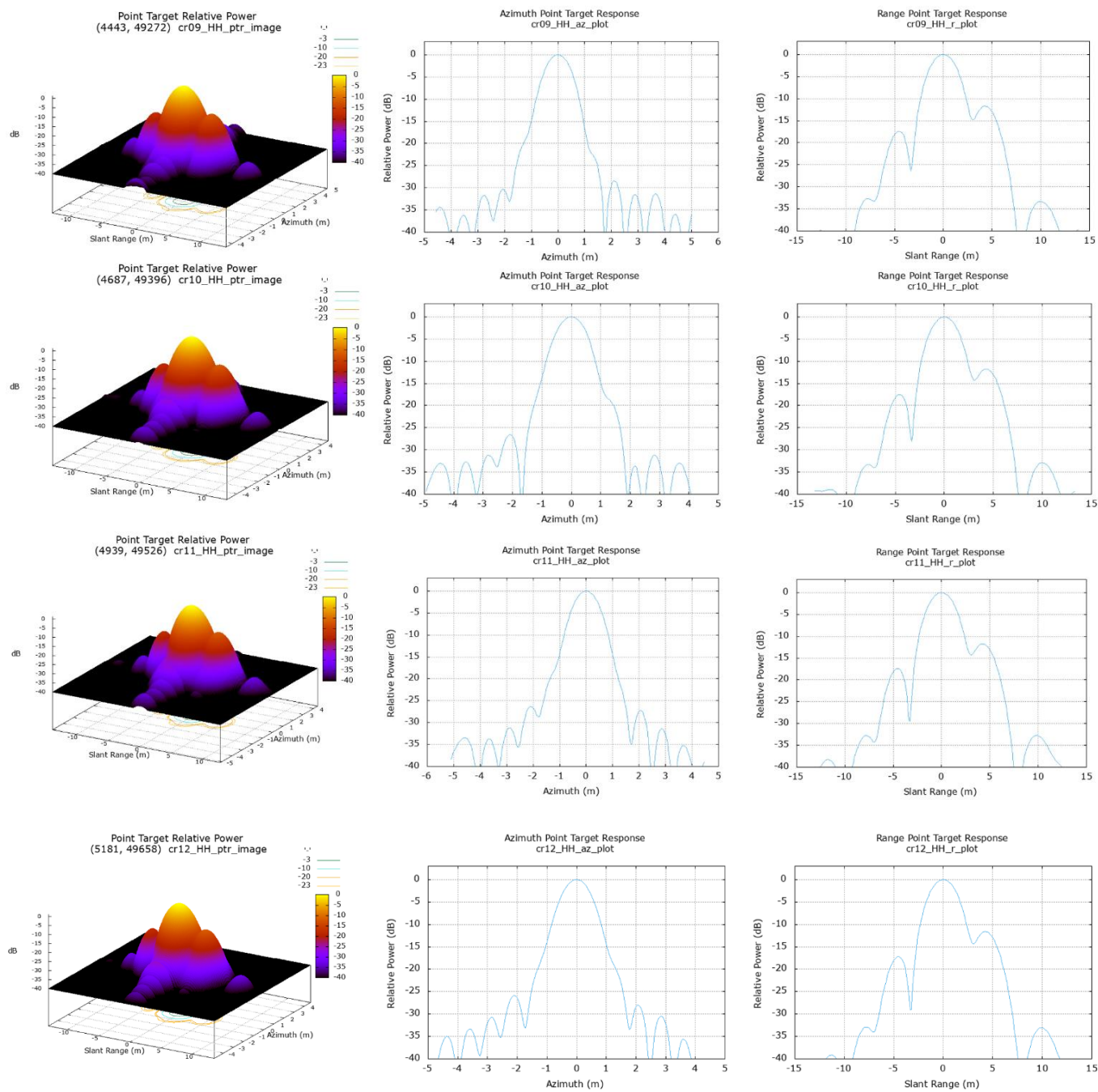
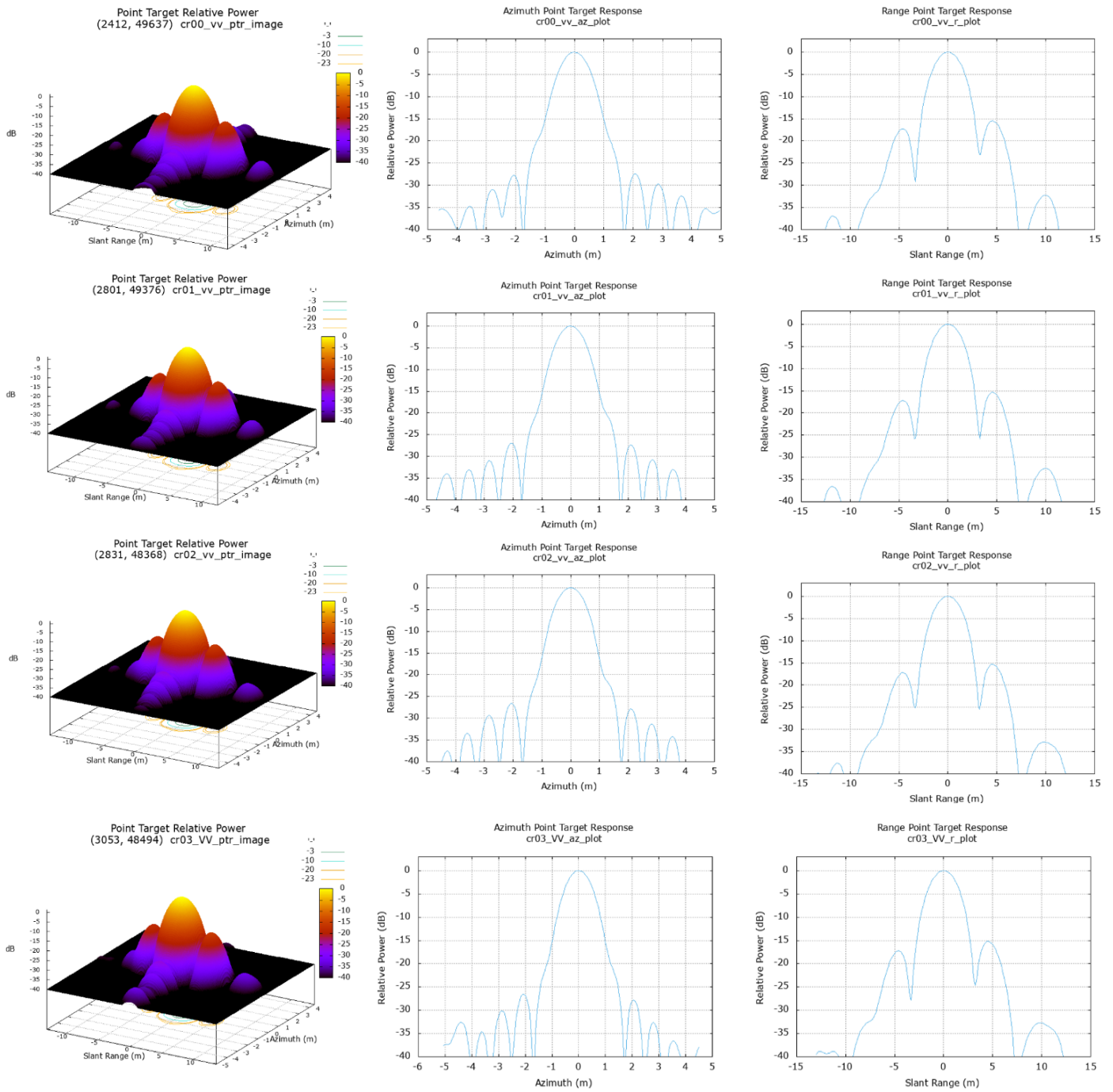
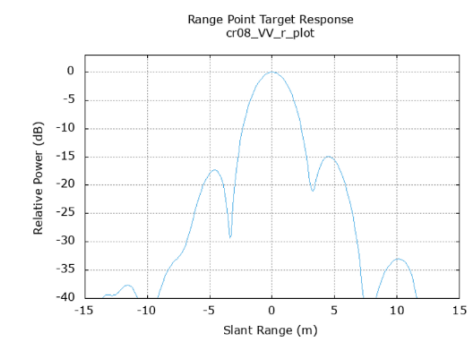
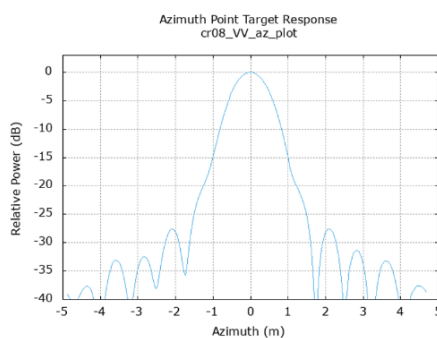
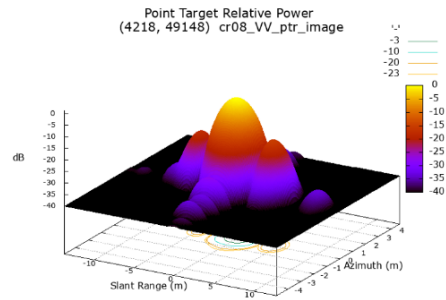
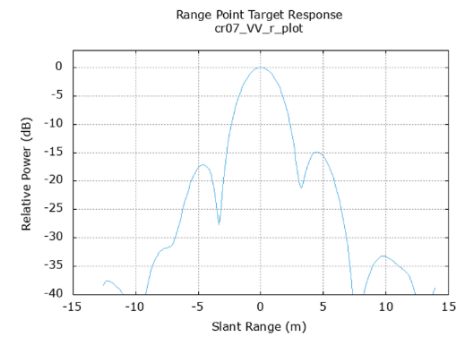
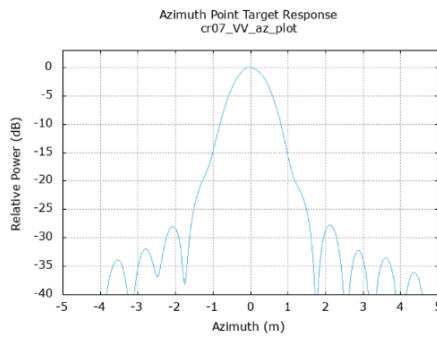
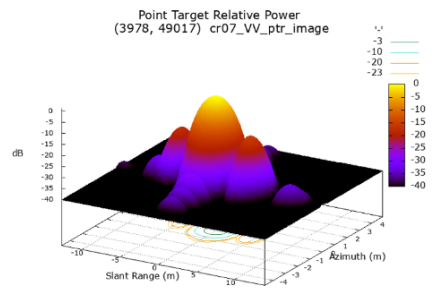
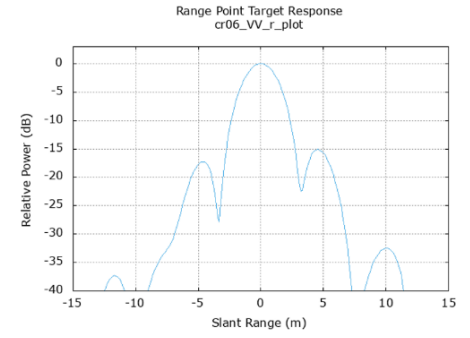
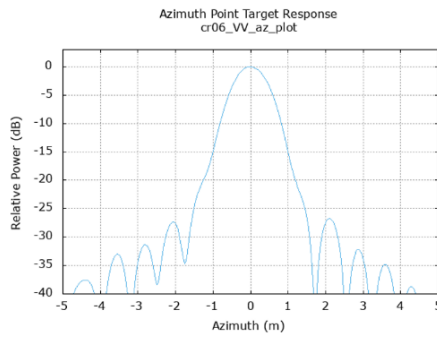
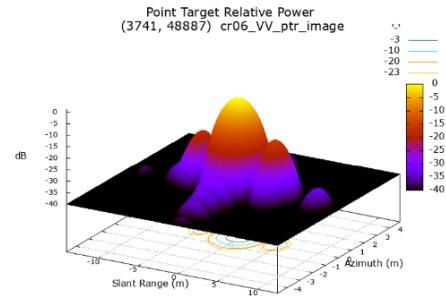
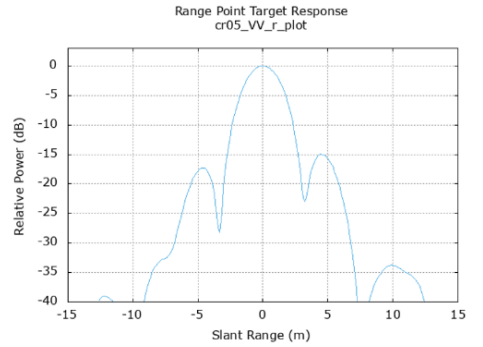
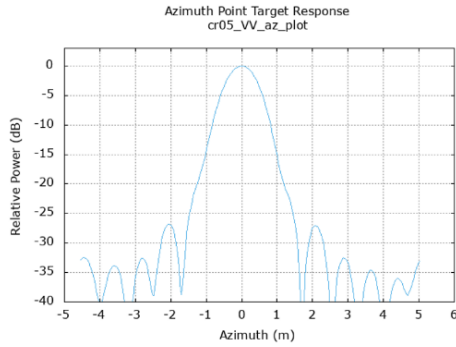
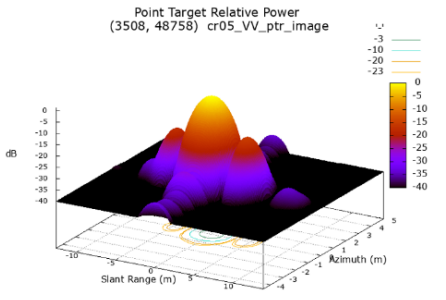
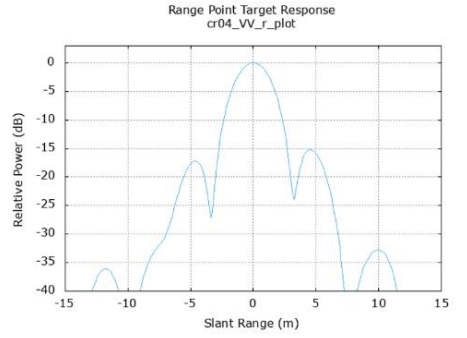
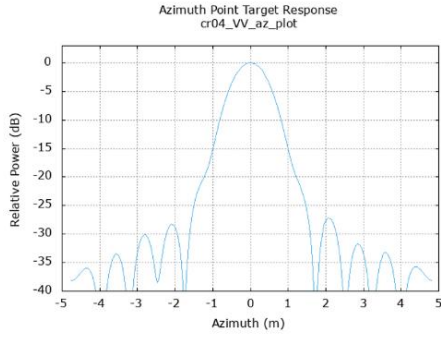
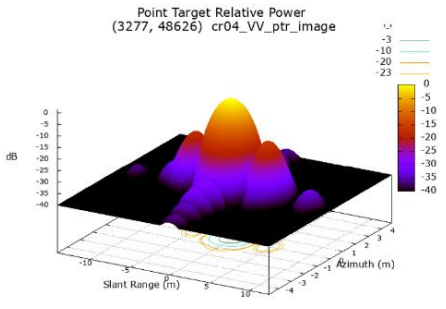


Figure 11. Impulse Response function of CR's using SLC image of HH pol

## 6.1.2 Impulse Response Functions for VV polarization





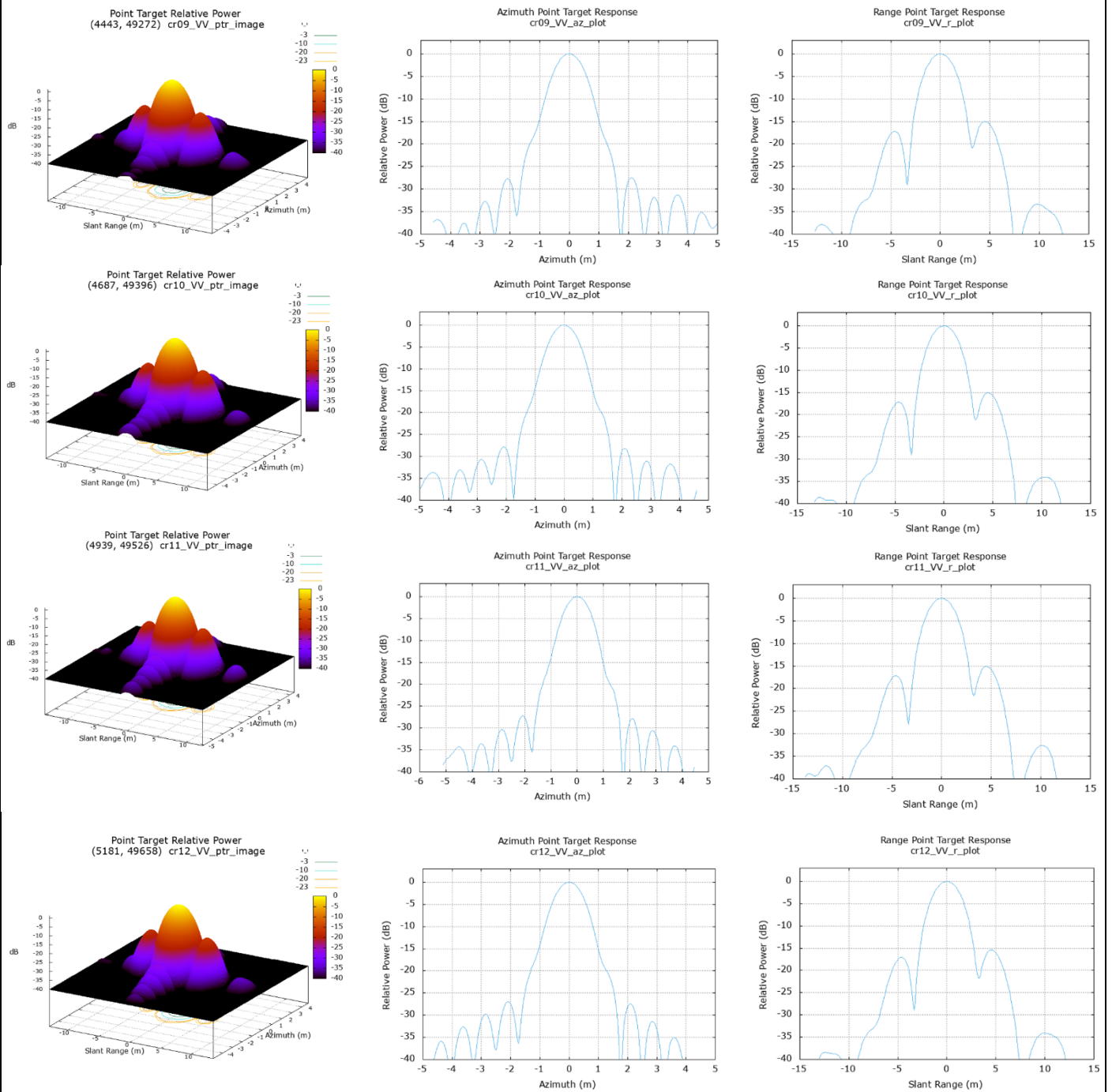


Figure 12. Impulse Response function of CR's using SLC image of VV pol

### 6.1.3 Channel Imbalance and Phase Bias

Co channel imbalance (f) for each corner reflector is estimated for HH and VV polarizations using Equation 14 and is given in Table 7. The mean value of them is considered as the effective value of f.

Table 6. Calculated Target Energy values after subtraction of clutter for quad pol

CR	Calculated target energy after subtraction of clutter in VV pol.(linear)	Calculated target energy after subtraction of clutter in HH pol. (linear)	Calculated target energy after subtraction of clutter in HV pol. (linear)	Calculated target energy after subtraction of clutter in VH pol. (linear)
<b>CR00</b>	2158.490	2158.580	18.735	6.823
<b>CR01</b>	2079.550	2146.040	81.108	72.689
<b>CR02</b>	2062.540	2210.050	44.210	22.612
<b>CR03</b>	2370.890	2029.640	97.339	77.731
<b>CR04</b>	1918.820	1854.290	12.140	13.374
<b>CR05</b>	1934.090	2193.250	59.399	30.442
<b>CR06</b>	1828.900	2221.110	19.363	5.970
<b>CR07</b>	1621.150	1920.410	30.010	15.669
<b>CR08</b>	1862.400	2106.120	18.984	6.530
<b>CR09</b>	1548.860	1645.380	22.868	12.513
<b>CR10</b>	1761.160	1671.560	44.520	26.256
<b>CR11</b>	1964.110	1950.120	27.016	52.985
<b>CR12</b>	2003.340	1797.610	58.701	70.584

Table 7. Estimation of co channel imbalance (f)

CR_id	Cal. Target energy after substr. Of clutter in VV (in linear)	Cal. Target energy after substr. Of clutter in HH (in linear)	square root of VV (in linear)	square root of HH (in linear)	Co-pol channel imbalance in linear (fi)
<b>CR00</b>	2158.490	2158.580	46.45955	46.46052	0.999979
<b>CR01</b>	2079.550	2146.040	45.60208	46.32537	0.984387

<b>CR02</b>	2062.540	2210.050	45.4152	47.01117	0.966051
<b>CR03</b>	2370.890	2029.640	48.69179	45.05153	1.080802
<b>CR04</b>	1918.820	1854.290	43.80434	43.06147	1.017251
<b>CR05</b>	1934.090	2193.250	43.97829	46.83215	0.939062
<b>CR06</b>	1828.900	2221.110	42.76564	47.12865	0.907423
<b>CR07</b>	1621.150	1920.410	40.26351	43.82248	0.918787
<b>CR08</b>	1862.400	2106.120	43.15553	45.89248	0.940362
<b>CR09</b>	1548.860	1645.380	39.35556	40.56328	0.970226
<b>CR10</b>	1761.160	1671.560	41.96618	40.88472	1.026451
<b>CR11</b>	1964.110	1950.120	44.31828	44.16016	1.003581
<b>CR12</b>	2003.340	1797.610	44.75869	42.39823	1.055673
				<i>Mean f in linear</i>	<b>0.985387</b>

Cross channel imbalance (g) is the difference between energy of a featureless homogenous patch estimated for HV and VH polarizations using Equation 16 and Equation 14. The estimated channel imbalance values is given by **Table 8**

Table 8. Estimation of cross channel imbalance (g)

<b>Values derived from SLC image using ENVI software</b>	<b>HV</b>	<b>VH</b>
Real	0.000011	0.000008
Imaginary	0.000026	0.000021
Amplitude (dB)	0.00002823119	0.000022472
Phase (dB)	1.17055567	1.20681737
<b><i>g (dB)</i></b>	<b><i>1.256271</i></b>	

Phase anomaly between co-channels of HH and VV polarization at each of the corner reflector  $\phi_t + \phi_r$  is estimated. The phase bias of co-channel  $\phi_s$  is estimated on each corner reflector using Equation 15. While for phase anomaly between cross channels –HV and VH  $\phi_t - \phi_r$  of featureless homogenous patch is estimated using Equation 17 and given by  $\phi_d$ .

The phase bias of co-channel and cross channel are estimated from  $\phi_s$  and  $\phi_d$  shown in Table 9

Table 9. Estimated Phase bias in transmitter and receiver for co-pol and cross-pol channels

	<b>In radians</b>	<b>In degrees</b>
$\mathbf{Phi}_d (\Phi_d)$	-0.03626	-2.077642
$\mathbf{Phi}_s (\Phi_s)$	0.027547	1.578333
$\mathbf{Phi}_t (\Phi_t)$	-0.00436	-0.249655
$\mathbf{Phi}_r(\Phi_r)$	0.031904	1.827988

#### 6.1.4 Polarimetric signatures after radiometric and phase correction

The radiometric and phase calibration correction has already applied for the dataset. Before radiometric and phase calibration the polarization signatures have double peaked nature due to  $180^\circ$  phase offset between the HH and VV channels. After correction the shapes of the polarimetric signatures at the corner reflector pixels should closely resemble the ideal shapes as shown in **Figure 13**. The polarization signatures generated using radiometric and phase corrected dataset are given in **Figure 14** (Alexander, Bruce and Brian 2014)

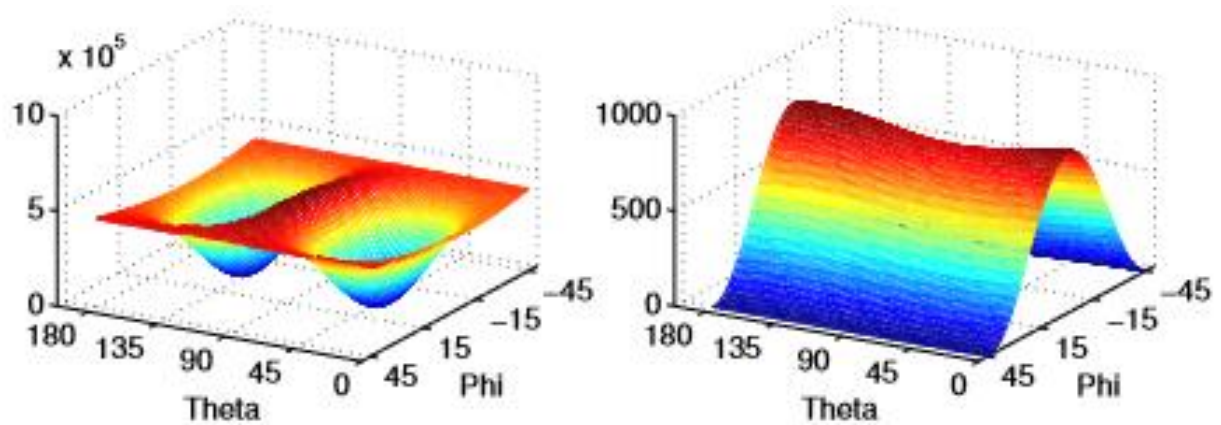


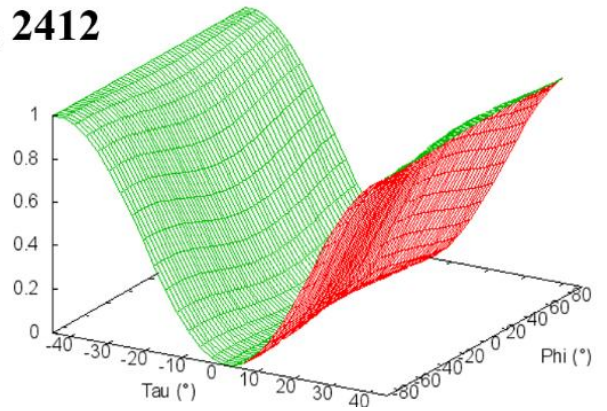
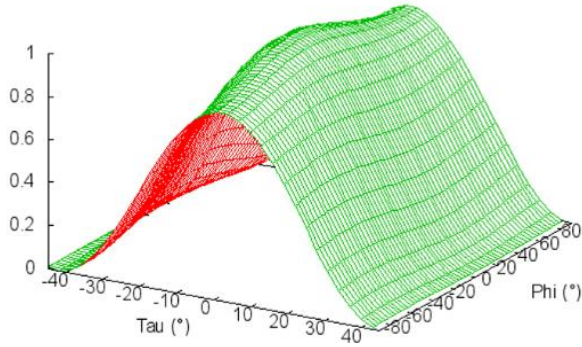
Figure 13. Polarimetric Signature of corner reflector in ideal case: Co-polarization signature of corner reflector before radiometric and phase calibration (left image); Co-polarization signature of corner reflector after radiometric and phase calibration (right image);©(Alexander, Bruce and Brian 2014)

## Polarimetric signatures from CR00- CR12

Normalized Polarimetric Signature : Co-polarisation channel

Normalized Polarimetric Signature : Cross-polarisation channel

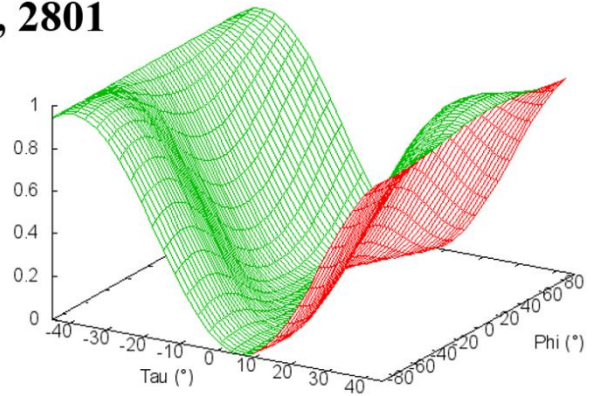
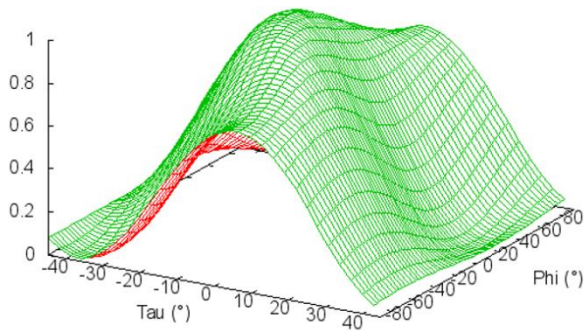
### CR00: 49637, 2412



Normalized Polarimetric Signature : Co-polarisation channel

Normalized Polarimetric Signature : Cross-polarisation channel

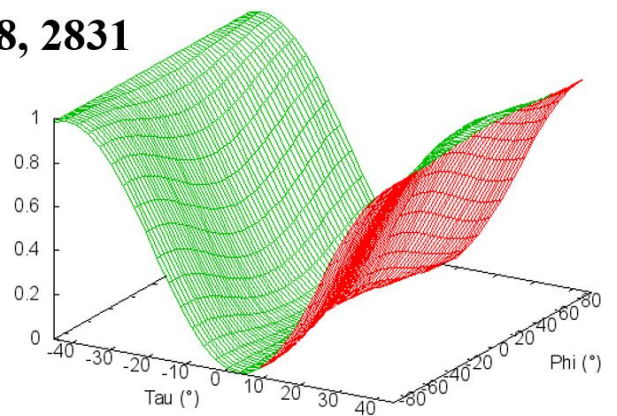
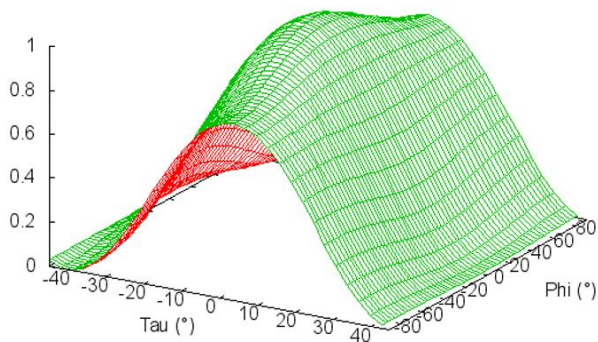
### CR01: 49376, 2801



Normalized Polarimetric Signature : Co-polarisation channel

Normalized Polarimetric Signature : Cross-polarisation channel

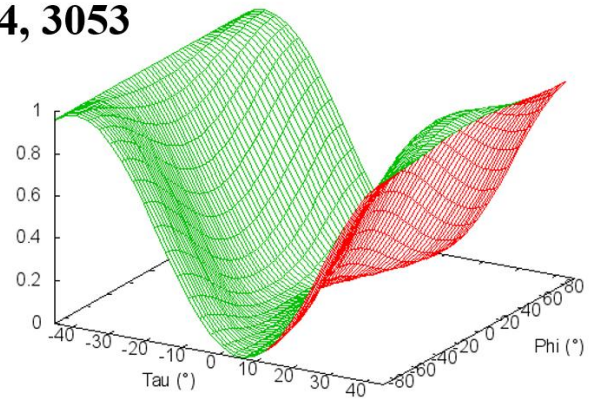
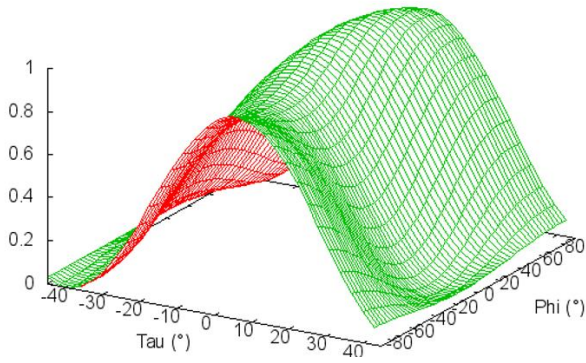
### CR02: 48368, 2831



Normalized Polarimetric Signature : Co-polarisation channel

Normalized Polarimetric Signature : Cross-polarisation channel

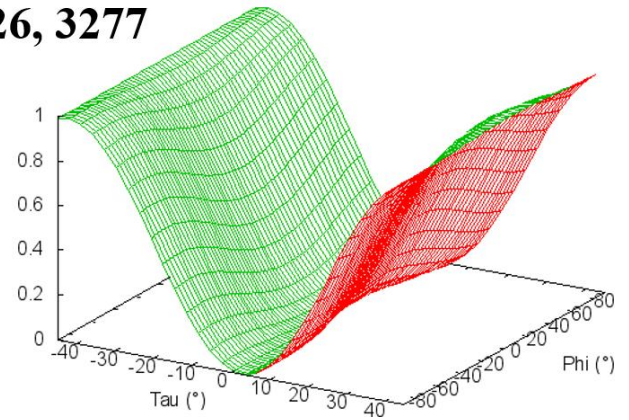
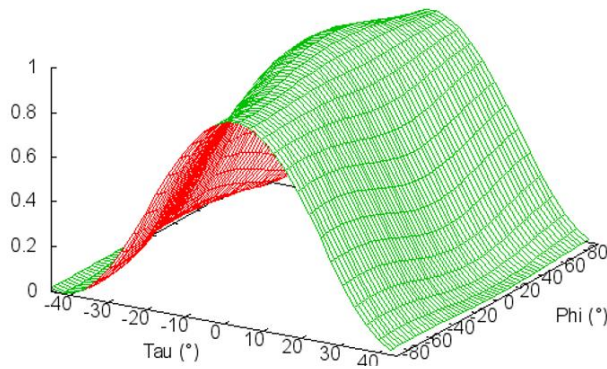
**CR03: 48494, 3053**



Normalized Polarimetric Signature : Co-polarisation channel

Normalized Polarimetric Signature : Cross-polarisation channel

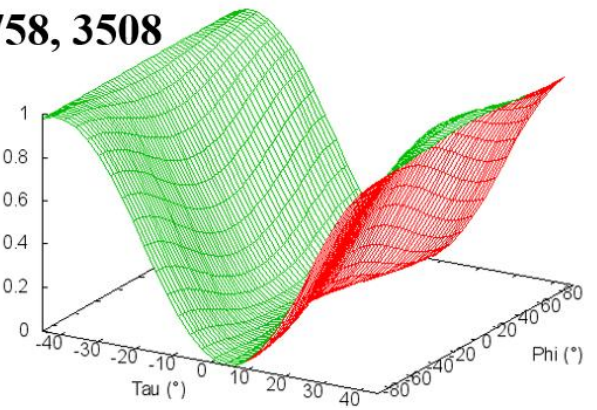
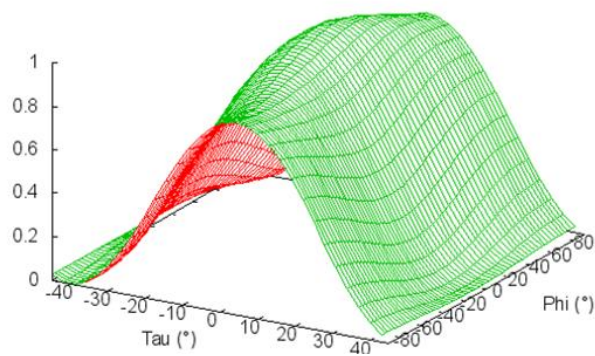
**CR04: 48626, 3277**



Normalized Polarimetric Signature : Co-polarisation channel

Normalized Polarimetric Signature : Cross-polarisation channel

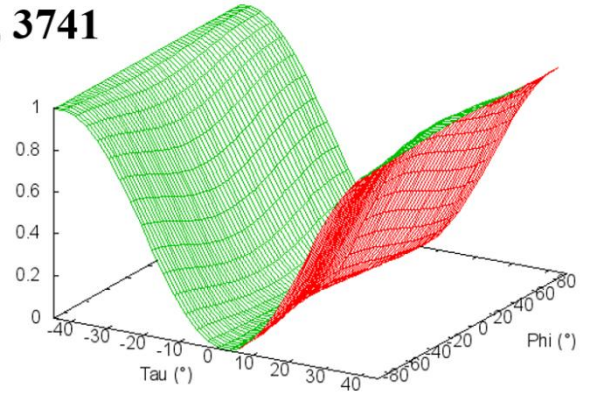
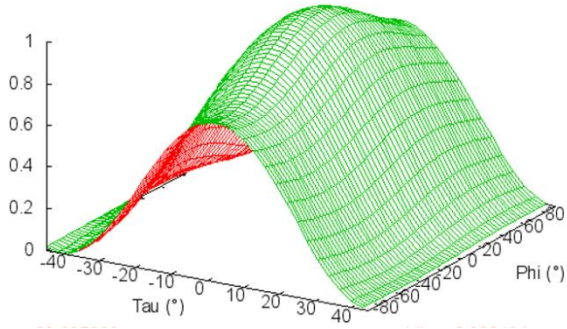
**CR05: 48758, 3508**



Normalized Polarimetric Signature : Co-polarisation channel

Normalized Polarimetric Signature : Cross-polarisation channel

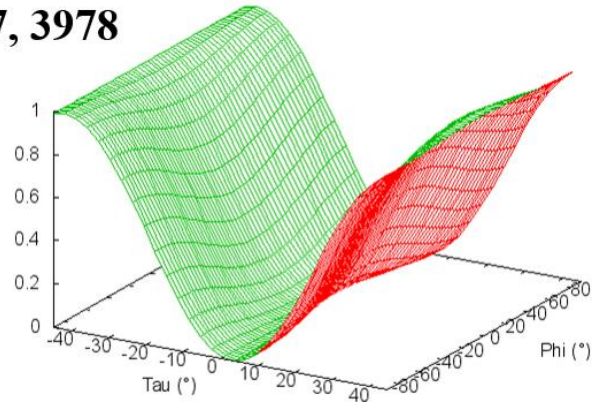
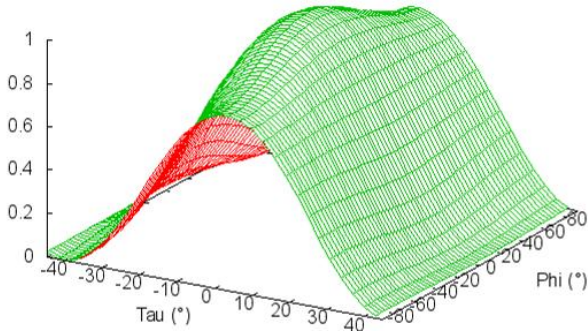
### CR06: 48887, 3741



Normalized Polarimetric Signature : Co-polarisation channel

Normalized Polarimetric Signature : Cross-polarisation channel

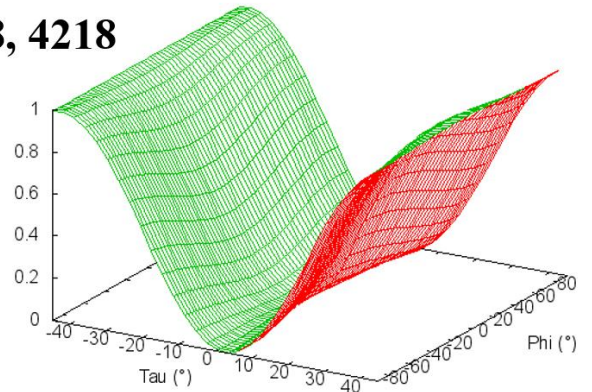
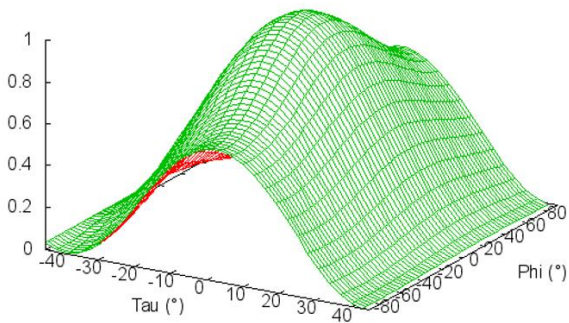
### CR07: 49017, 3978



Normalized Polarimetric Signature : Co-polarisation channel

Normalized Polarimetric Signature : Cross-polarisation channel

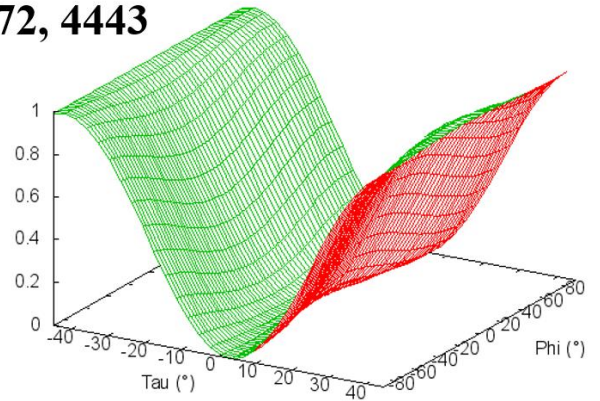
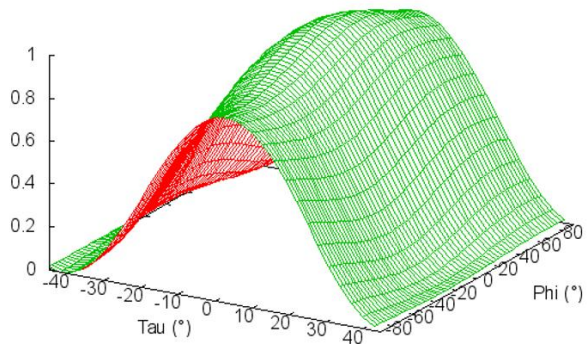
### CR08: 49148, 4218



Normalized Polarimetric Signature : Co-polarisation channel

Normalized Polarimetric Signature : Cross-polarisation channel

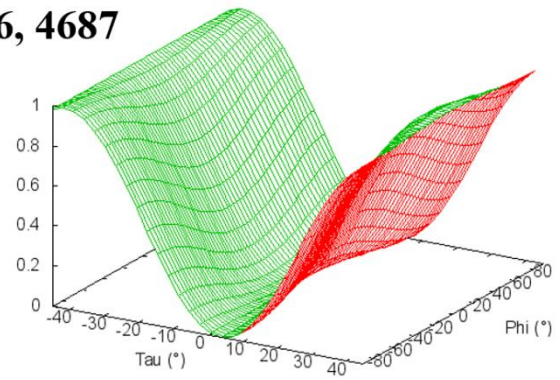
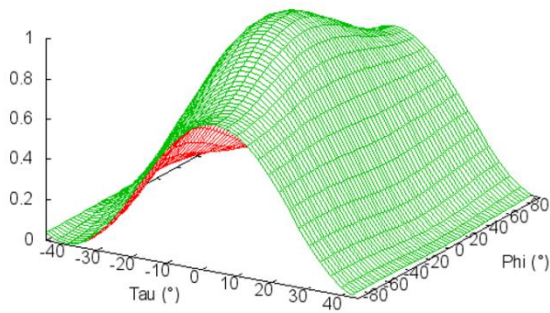
**CR09: 49272, 4443**



Normalized Polarimetric Signature : Co-polarisation channel

Normalized Polarimetric Signature : Cross-polarisation channel

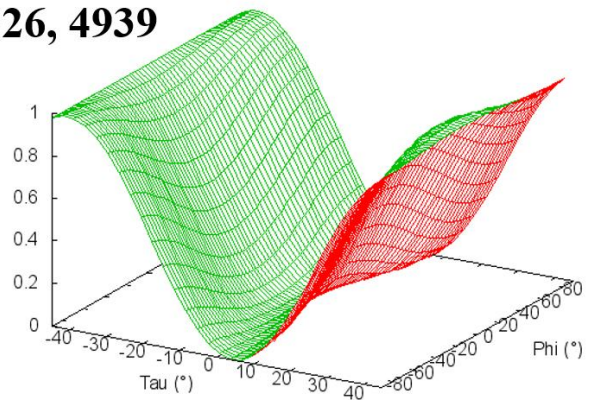
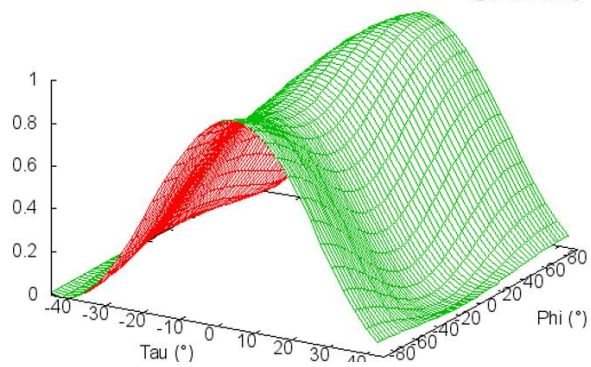
**CR10: 49396, 4687**



Normalized Polarimetric Signature : Co-polarisation channel

Normalized Polarimetric Signature : Cross-polarisation channel

**CR11: 49526, 4939**



Normalized Polarimetric Signature : Co-polarisation channel

Normalized Polarimetric Signature : Cross-polarisation channel

**CR12: 49658, 5181**

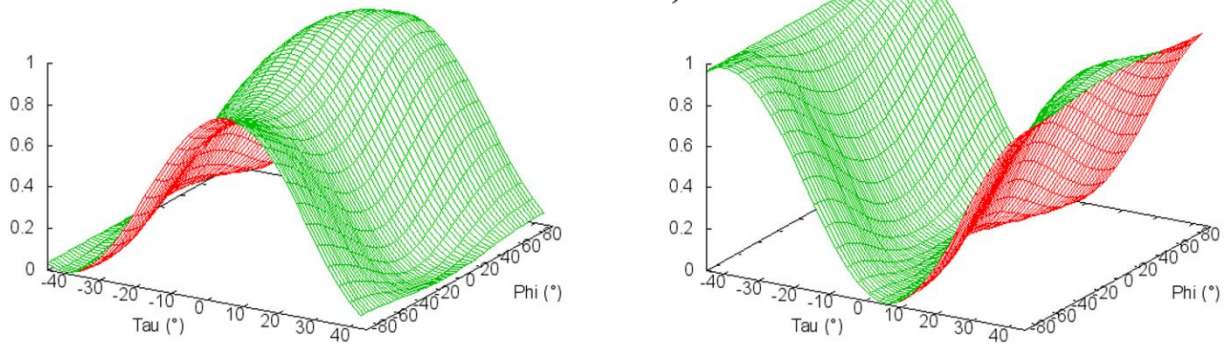


Figure 14. Polarimetric Signatures of Triangular Trihedral Corner Reflector after Radiometric and Phase Calibration

The polarimetric signatures of the 2.4 m corner reflectors are shown in **Figure 14**, which closely depict the ideal shape of the triangular trihedral corner reflector. The phase offset is reasonable and even though there are some visible distortions in the co-pol and cross-pol signatures generated for the corner reflector, the distortions are not high. Therefore, the dataset is radiometrically calibrated and the presence of phase bias is negligible.

## 6.2 Polarization parameters

The above methodology in the above sections generate SLC data that are radiometrically and phase calibrated dataset. This dataset contains residual cross talks and channel imbalances of the polarization channels. This partial calibrated dataset is used as the input for polarimetric correction. This correction excludes cross talk calibration while maintaining radiometric and phase calibration.

### 6.2.1 Impulse Response Function for HV polarization

The well cross talk calibrated dataset shouldn't have target energy in cross polarized channels. But in this dataset the presence of corner reflectors is clearly visible in the SLC image of cross polarized data as show in **Figure 15**. This is also due to cross talks and channels

imbalance errors. Hence cross talk and channel imbalance correction is required for this dataset. The impulse response for each corner reflector is generated and shown in **Figure 16**.

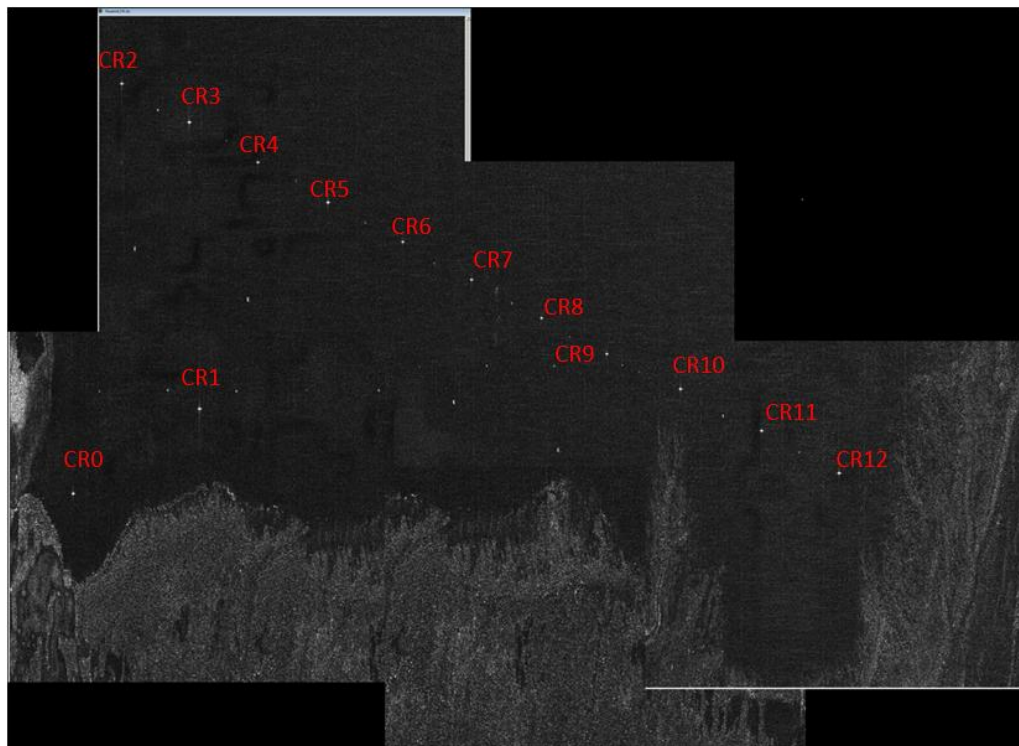
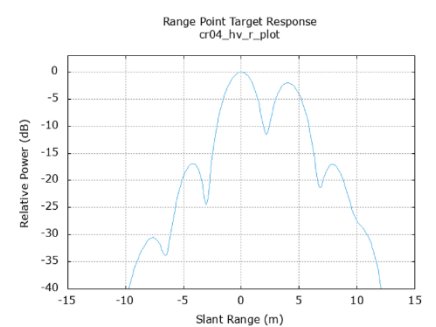
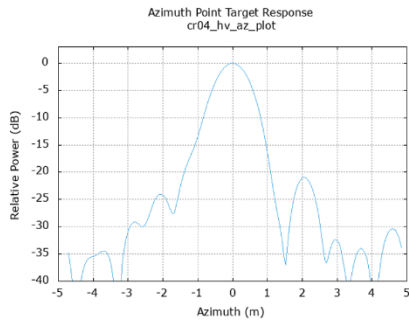
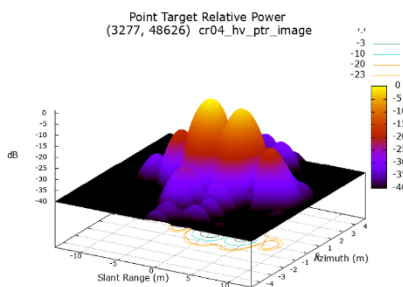
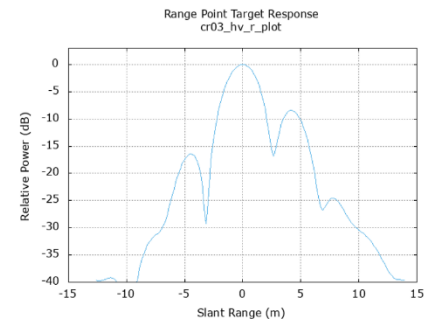
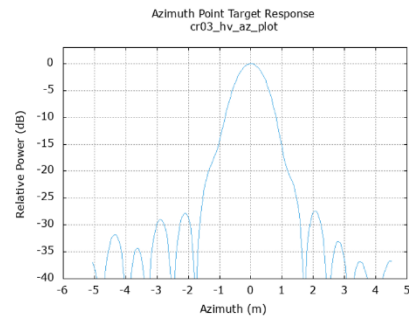
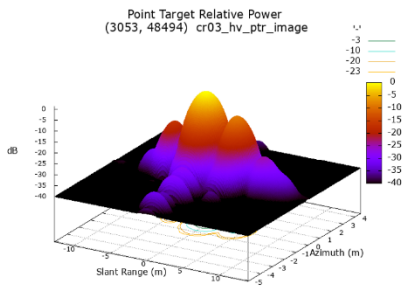
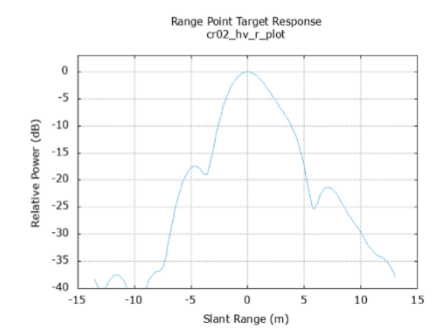
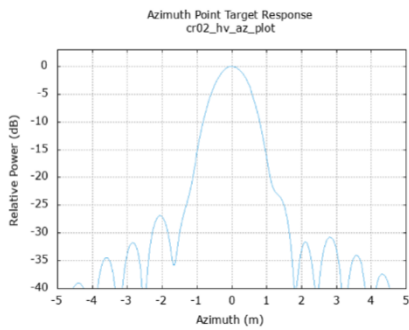
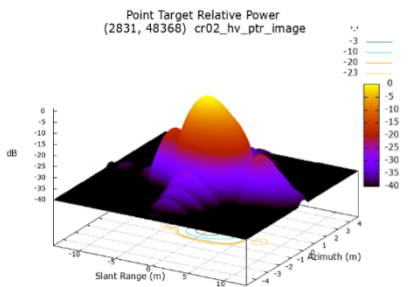
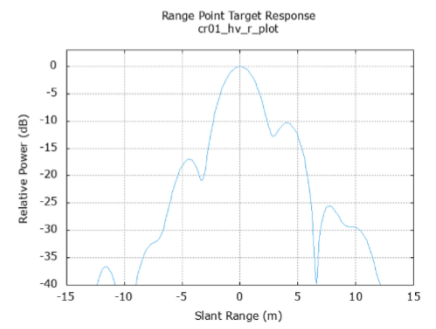
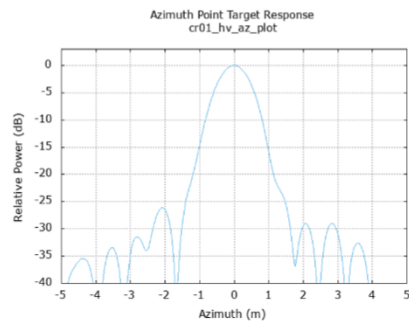
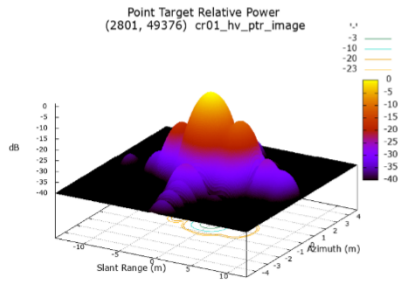
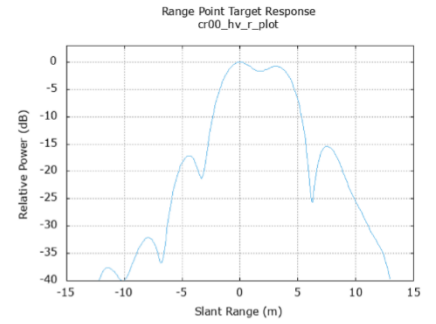
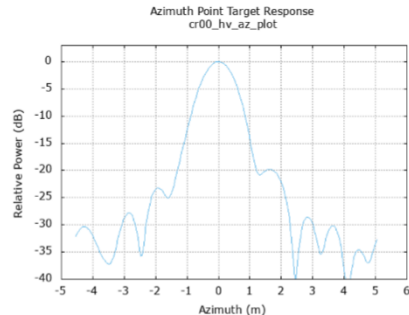
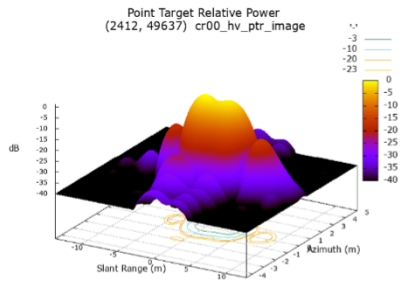
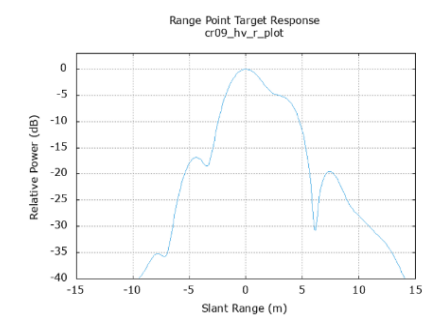
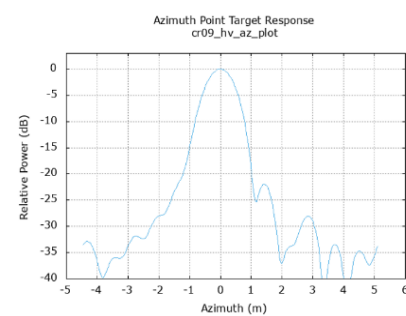
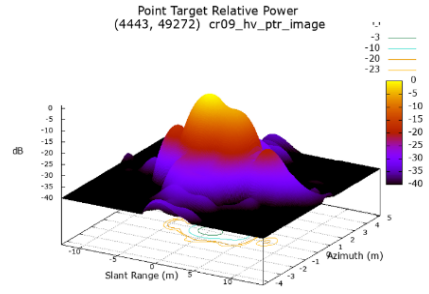
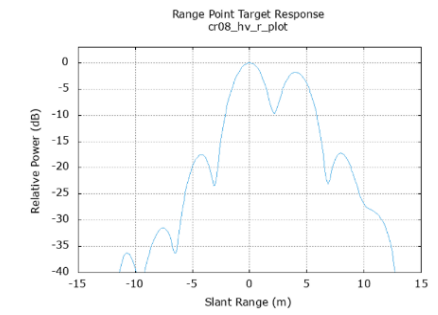
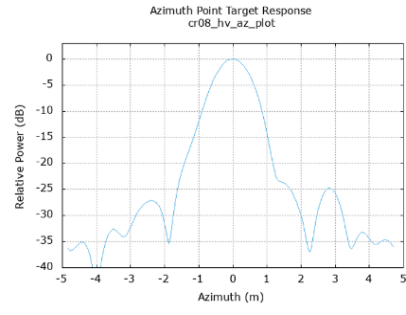
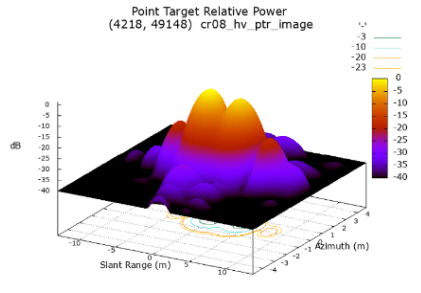
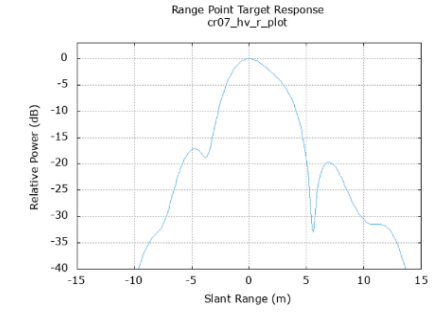
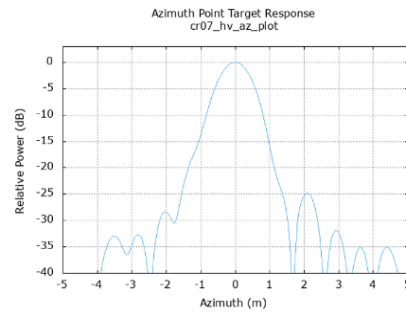
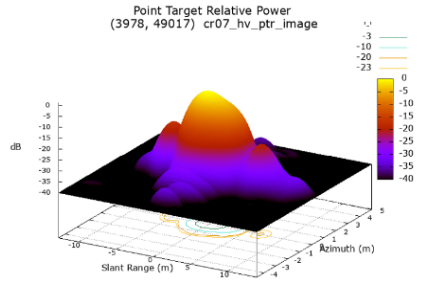
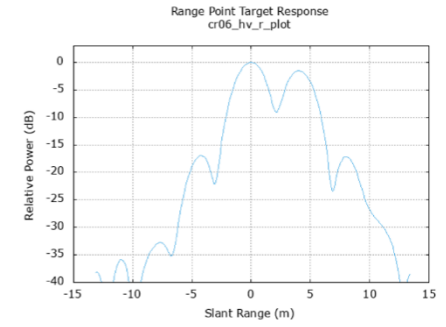
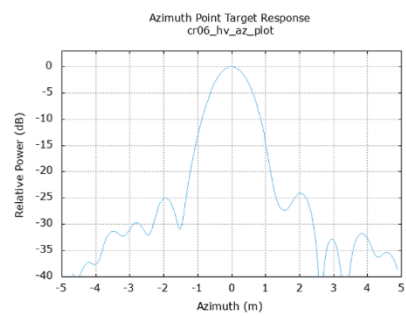
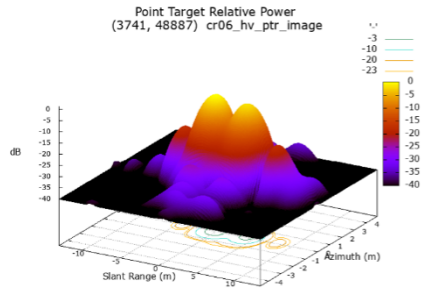
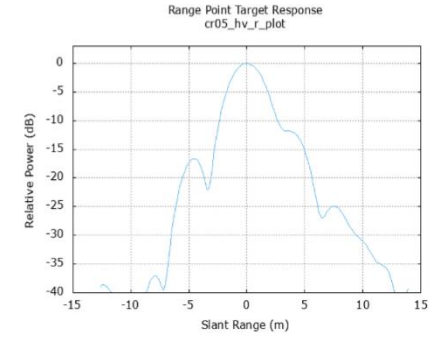
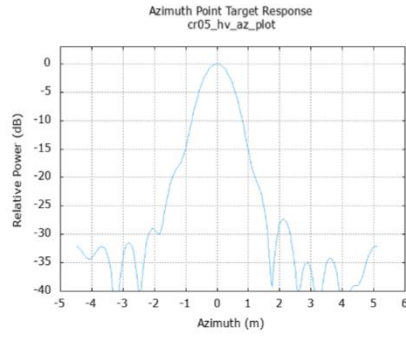
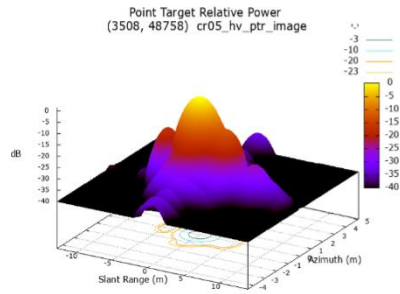


Figure 15. Location of CR's in SLC image of HV pol





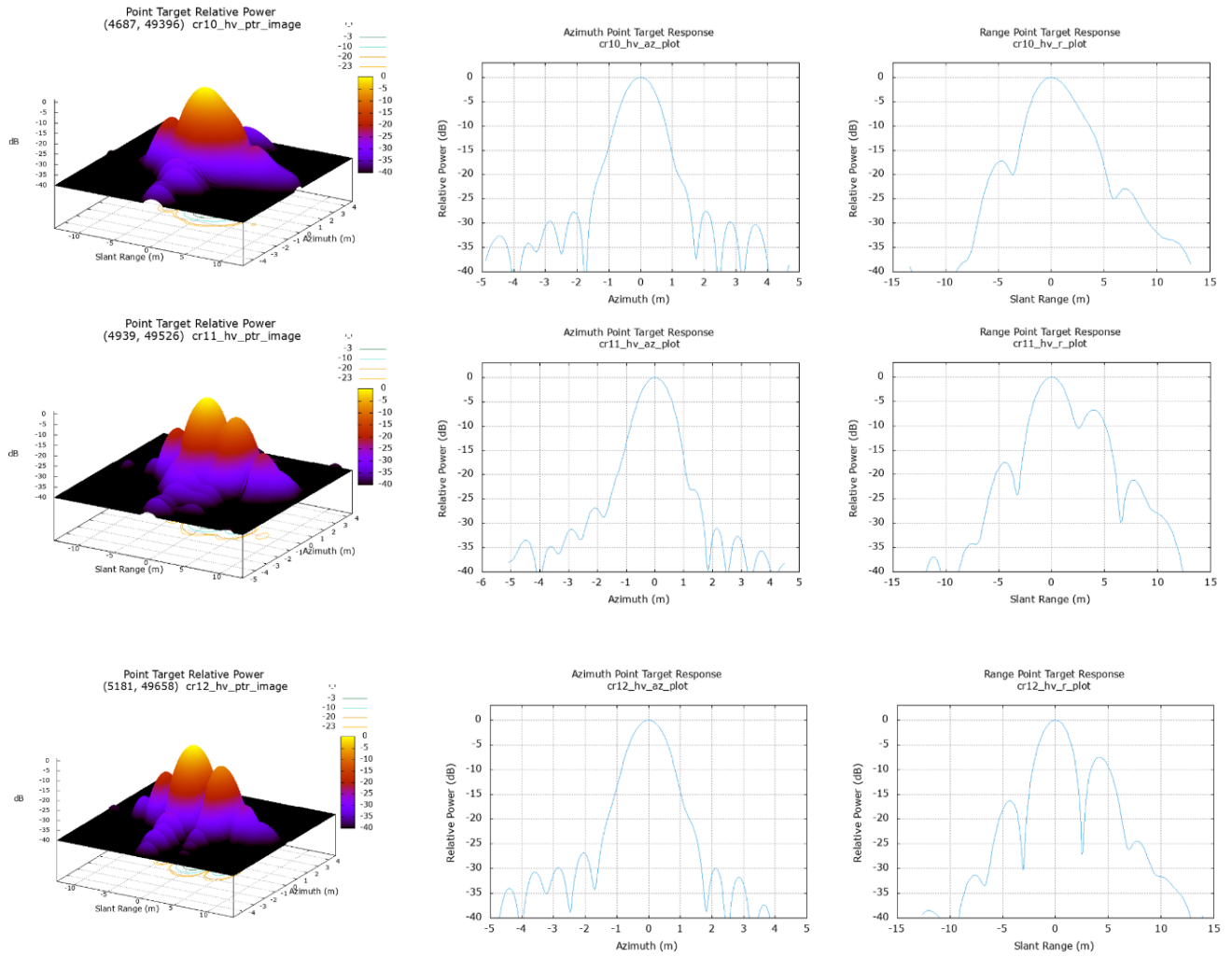


Figure 16. Impulse Response of CR using SLC image of HV

### 6.2.2 Estimation of cross talk and channel imbalance by Quegan's Method

Using Quegan algorithm the following cross talk and channels imbalance parameters are estimated with the procedure mentioned in above section 5.2. The estimated cross talk and channel imbalances for dataset in given in the **Table 10** and its contains absolute amplitude values in linear form.

Table 10. Estimation of cross talk and channel imbalance using Quegan algorithm

	u_abs (linear)	v_abs (linear)	z_abs (linear)	w_abs (linear)	alpha_abs (linear)
CR00	2.2547	4.7745	2.9872	5.7732	0.7884
CR01	0.5634	1.2853	0.4756	1.1738	1.461
CR02	0.5246	1.1457	3.2758	5.5407	0.1754
CR03	0.4214	1.6154	0.2978	0.8121	3.2765
CR04	0.2088	0.4691	0.6816	1.9522	0.3553
CR05	0.9832	0.6207	0.3574	0.3387	0.8972
CR06	0.1394	0.6383	0.073	0.9152	0.9781
CR07	1.9697	1.9171	2.6269	2.6188	0.754
CR08	0.0019	0.9061	0.0011	0.3821	1
CR09	4.5734	4.4968	4.6416	4.4497	1.0103
CR10	0.1707	0.3853	0.1106	0.3303	1
CR11	0.0158	0.1181	5.16E-06	0.4141	219.049
CR12	0.2365	0.333	2.4281	2.5775	0.4084

### 6.3 Polarimetric Signatures- GRD Data

Polarimetric signatures are generated for the same study area dry lake, Rosamond using ground range detected (GRD) of quad polarization data. The covariance matrix of 3x3 form is used to generate the signatures which is radiometric and polarimetric corrected dataset. The ideal polarimetric signature of the corner reflector for co-pol and cross-pol channel is shown in **Figure 17**, the estimated signatures in this section should match with ideal case.

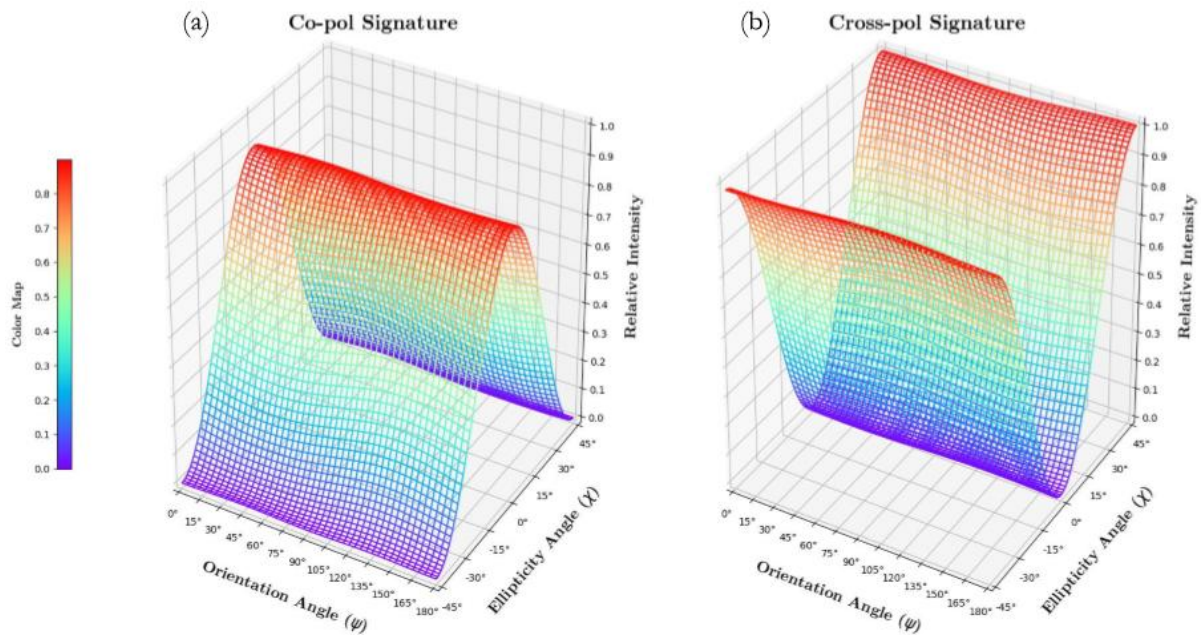
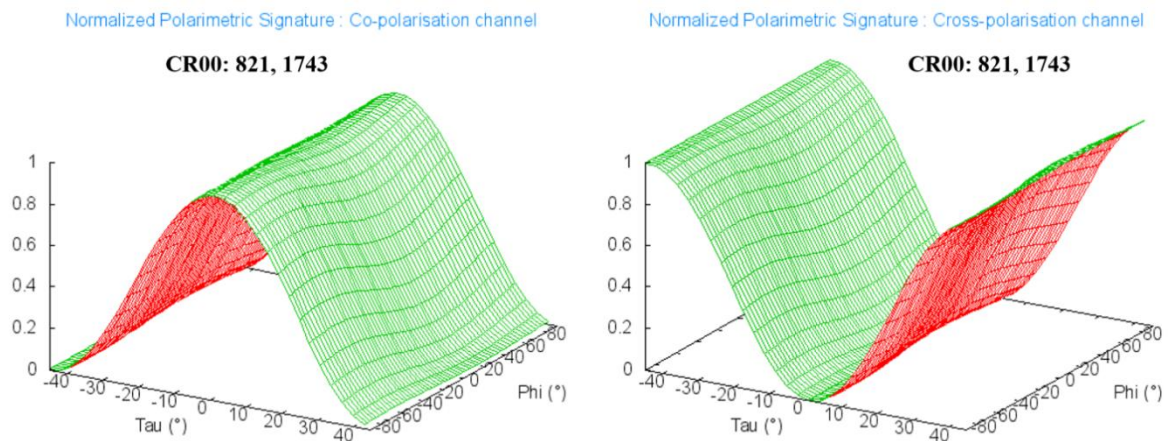


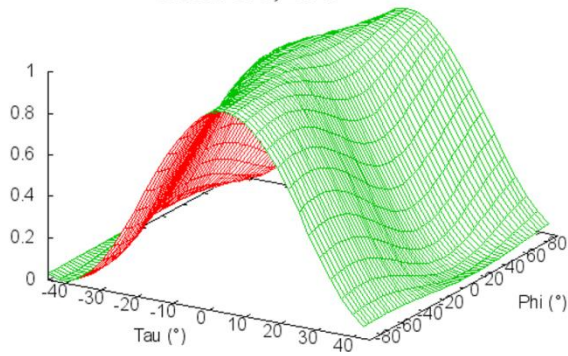
Figure 17. Polarimetric signature of triangular trihedral corner reflector (ideal case) © (Abhisek, Shashi and Valentyn 2019)

### Polarimetric signature of triangular trihedral corner reflector



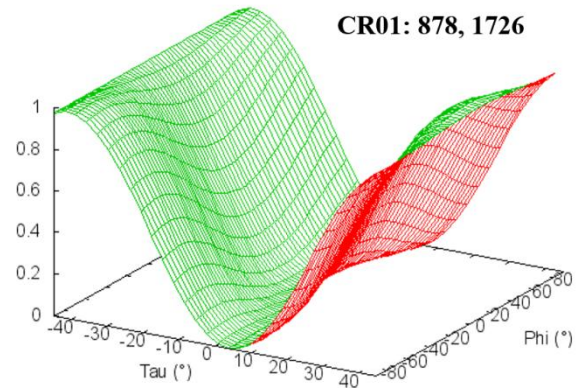
Normalized Polarimetric Signature : Co-polarisation channel

**CR01: 878, 1726**



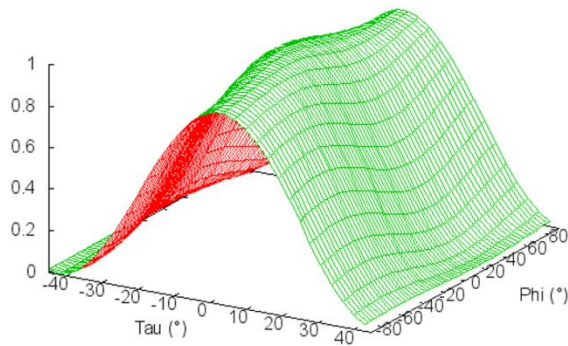
Normalized Polarimetric Signature : Cross-polarisation channel

**CR01: 878, 1726**



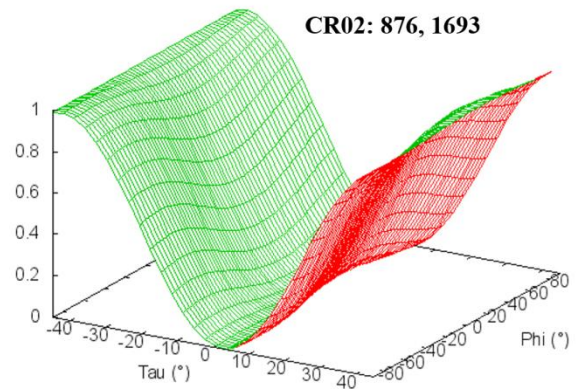
Normalized Polarimetric Signature : Co-polarisation channel

**CR02: 876, 1693**



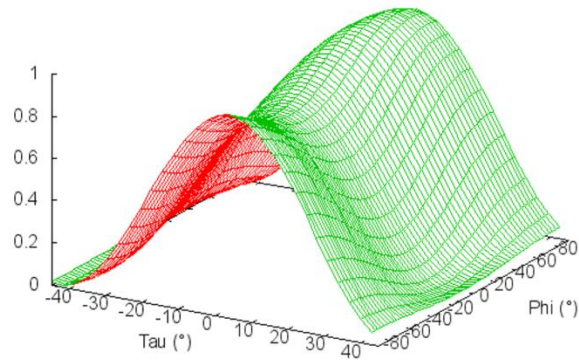
Normalized Polarimetric Signature : Cross-polarisation channel

**CR02: 876, 1693**



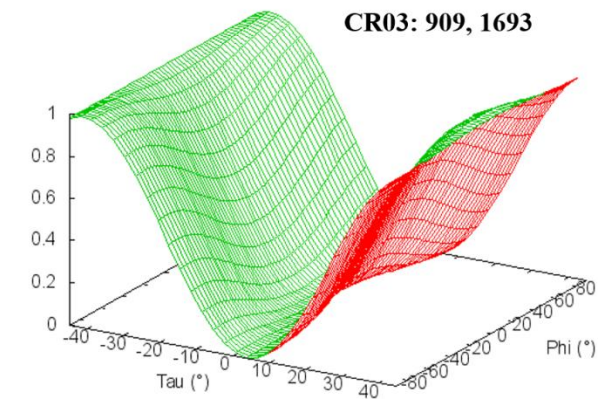
Normalized Polarimetric Signature : Co-polarisation channel

**CR03: 909, 1693**



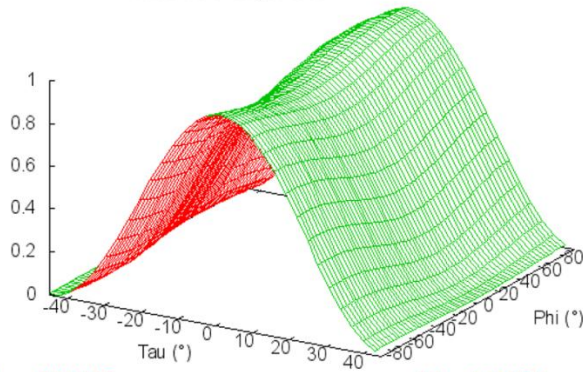
Normalized Polarimetric Signature : Cross-polarisation channel

**CR03: 909, 1693**



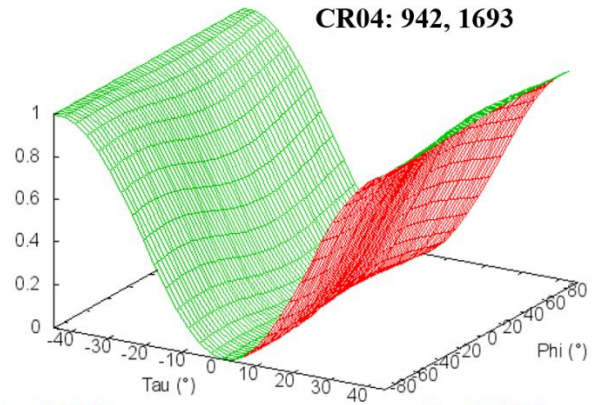
Normalized Polarimetric Signature : Co-polarisation channel

**CR04: 942, 1693**



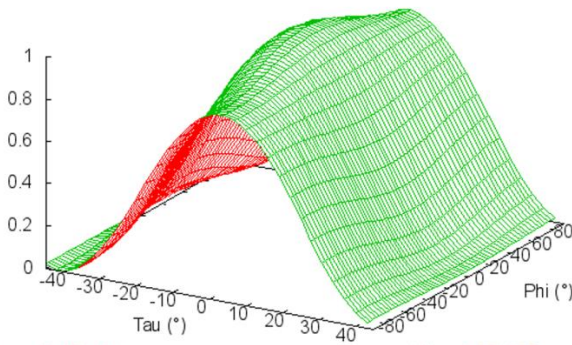
Normalized Polarimetric Signature : Cross-polarisation channel

**CR04: 942, 1693**



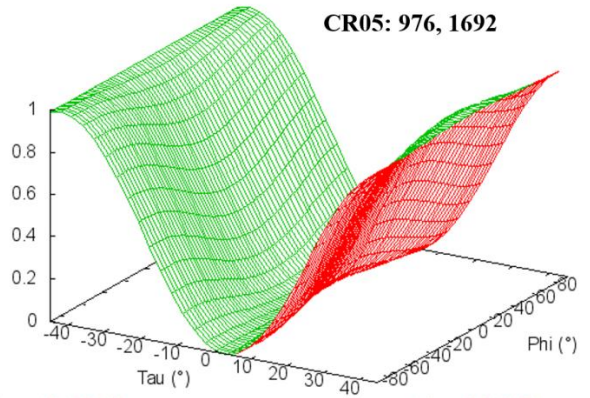
Normalized Polarimetric Signature : Co-polarisation channel

**CR05: 976, 1692**



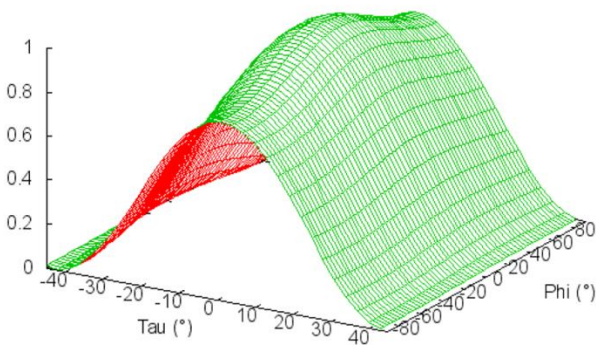
Normalized Polarimetric Signature : Cross-polarisation channel

**CR05: 976, 1692**



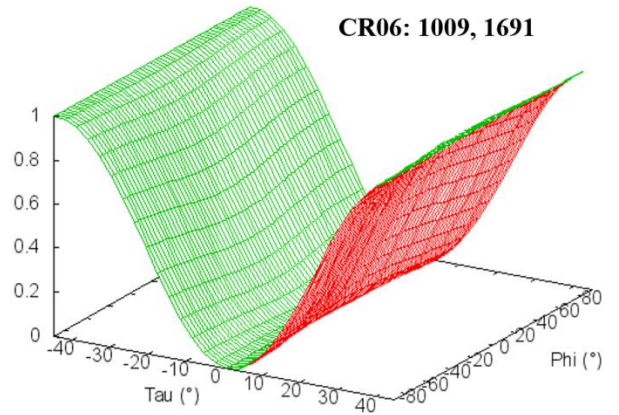
Normalized Polarimetric Signature : Co-polarisation channel

**CR06: 1009, 1691**



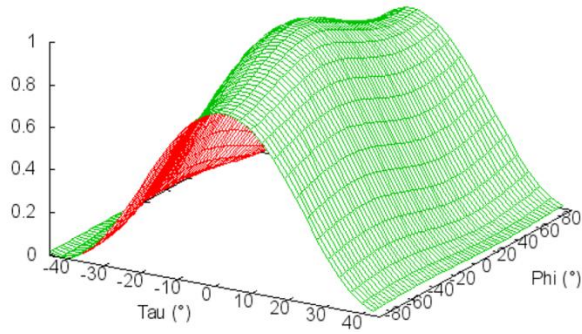
Normalized Polarimetric Signature : Cross-polarisation channel

**CR06: 1009, 1691**



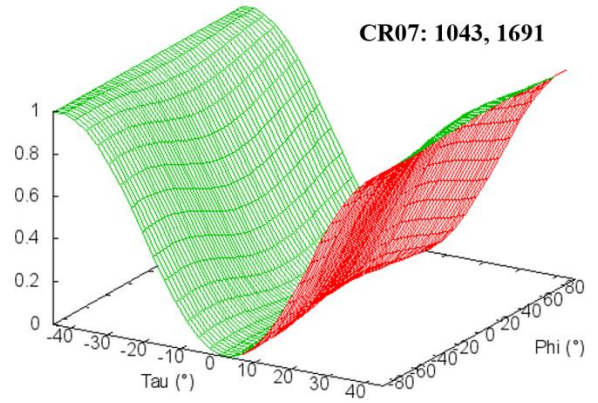
Normalized Polarimetric Signature : Co-polarisation channel

**CR07: 1043, 1691**



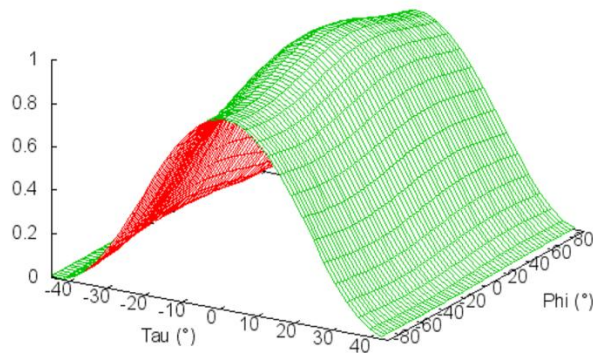
Normalized Polarimetric Signature : Cross-polarisation channel

**CR07: 1043, 1691**



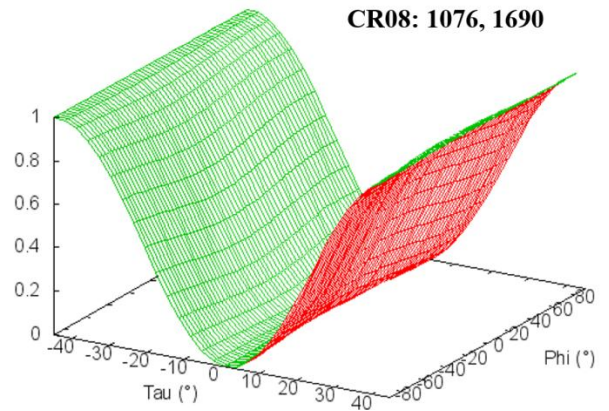
Normalized Polarimetric Signature : Co-polarisation channel

**CR08: 1076, 1690**



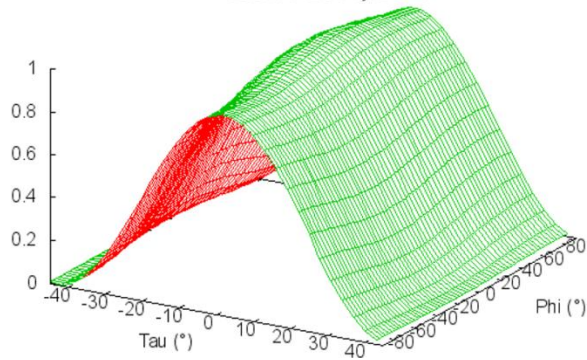
Normalized Polarimetric Signature : Cross-polarisation channel

**CR08: 1076, 1690**



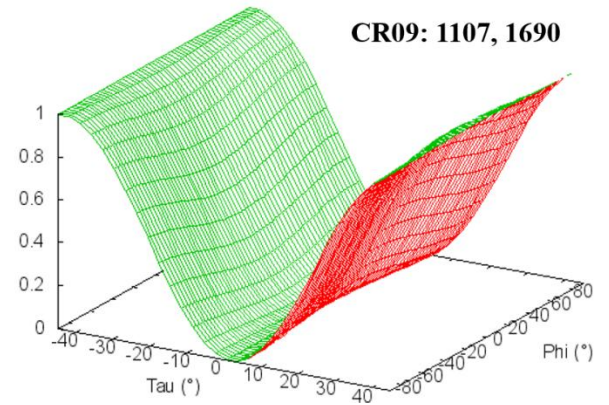
Normalized Polarimetric Signature : Co-polarisation channel

**CR09: 1107, 1690**



Normalized Polarimetric Signature : Cross-polarisation channel

**CR09: 1107, 1690**



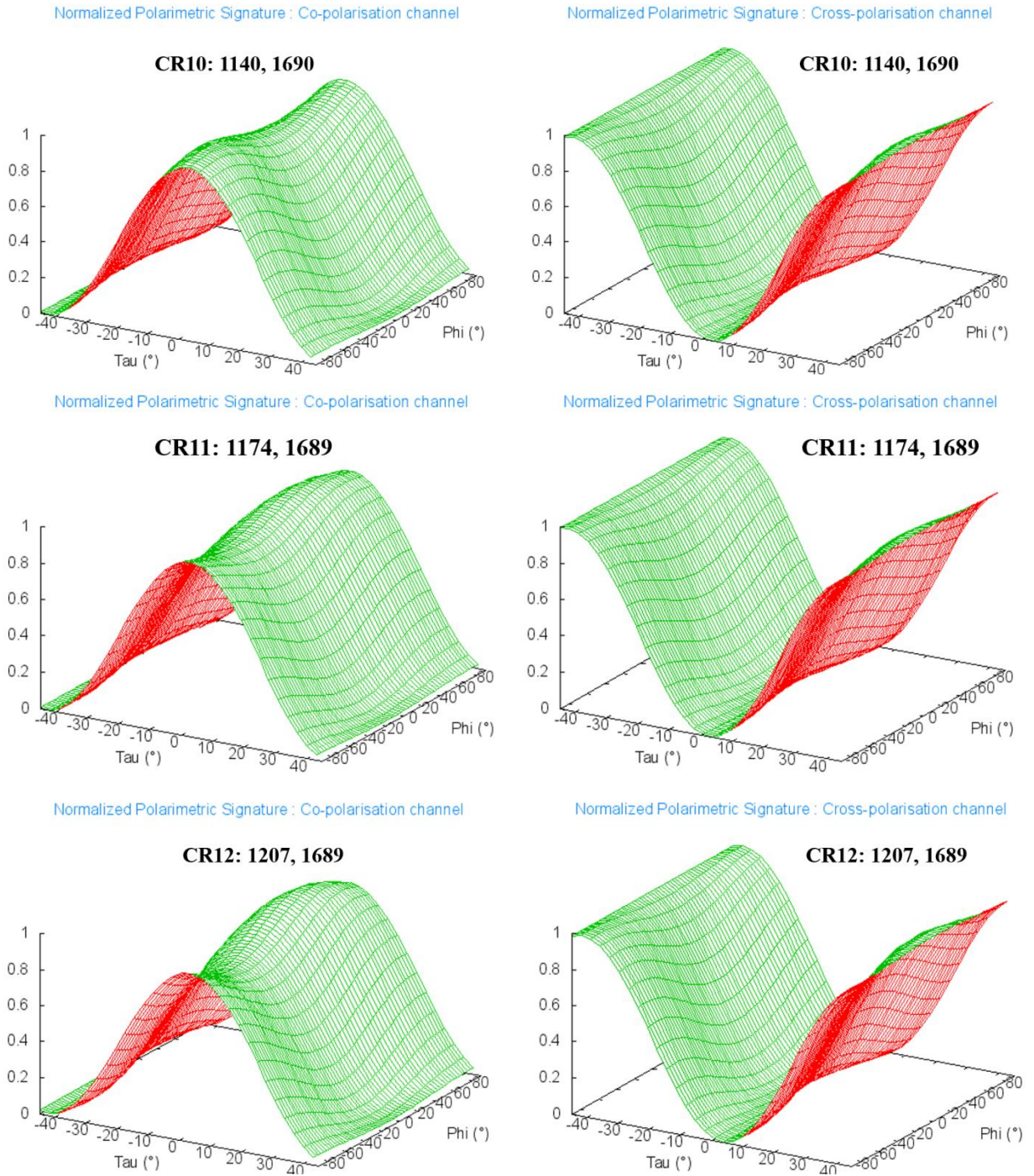


Figure 18. polarimetric signatures of each CR after cross talk and channel imbalance calibration

The above generated polarimetric signatures match with ideal signature and there are no visible distortions in signatures. The GRD dataset is well corrected for cross talk and channel imbalances.

6.4 Opportunistic Targets- Windmills present in the UAVSAR L band SLC  
data

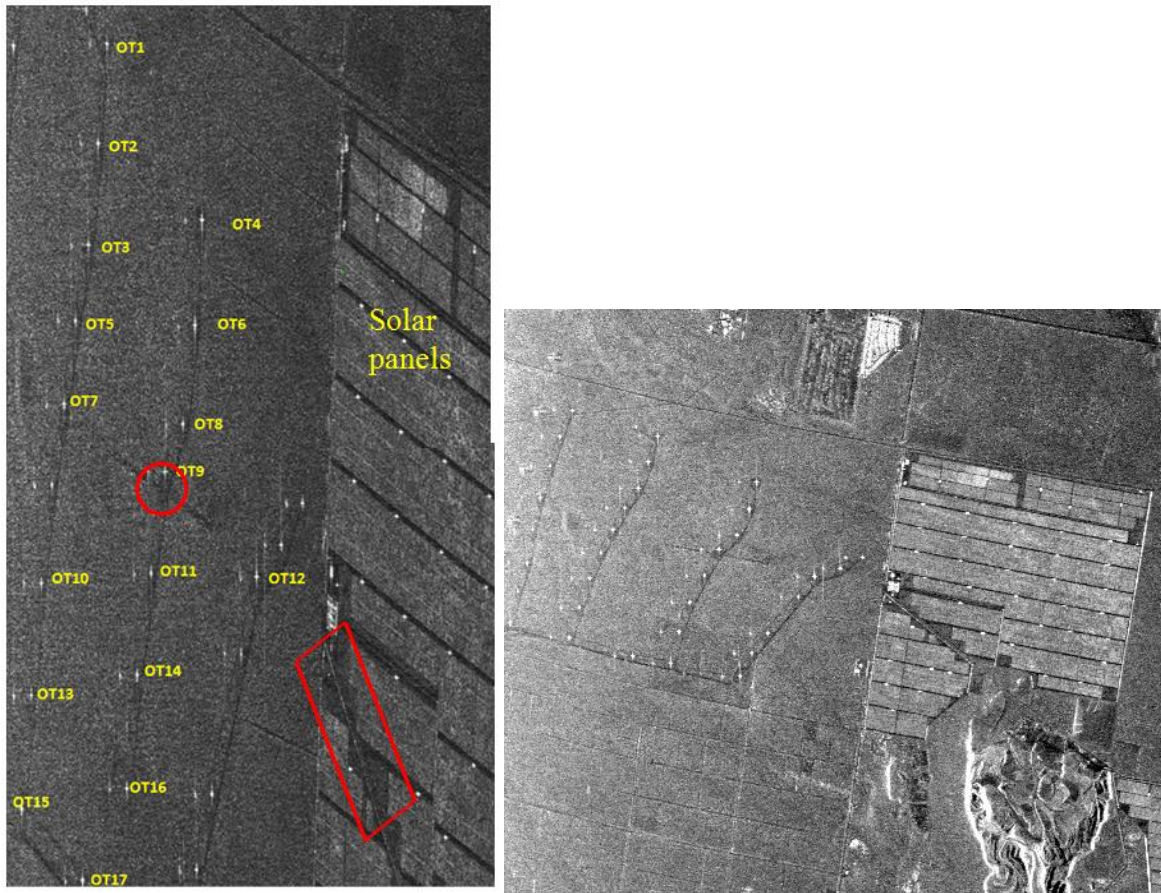


Figure 19. Above fig. are SLC (left); MLC (right) tile of UAVSAR L band data showing windmills

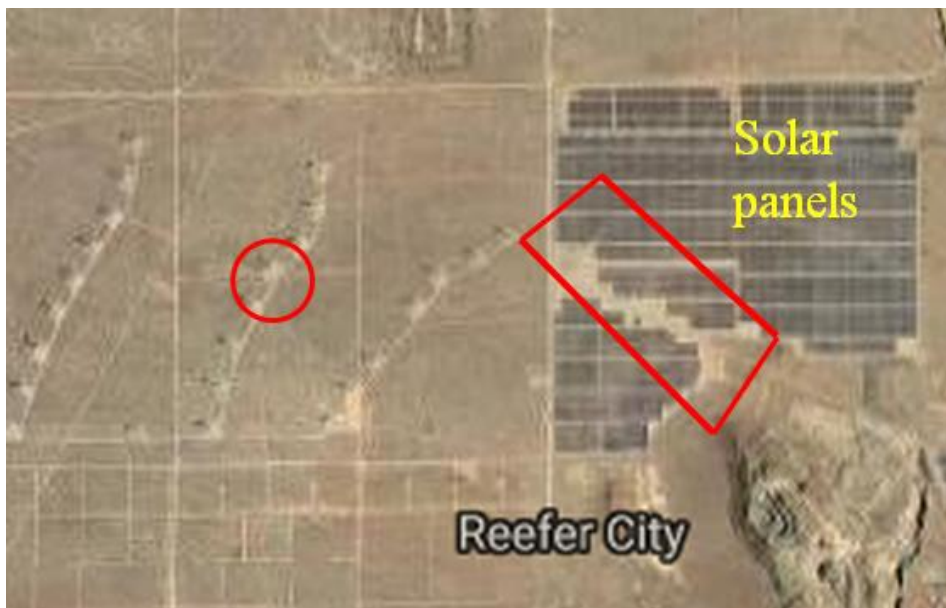


Figure 20. showing windmills in Google Earth image

In this study we used windmills as opportunistic targets for validation of azimuth and range resolutions. The above Figure 19 and Figure 20 shows the windmills which are visible in the SLC, Multi look data and Google earth image for verification of them.

Table 11 Range and Azimuth resolution at 3dB width using opportunistic targets (windmills)

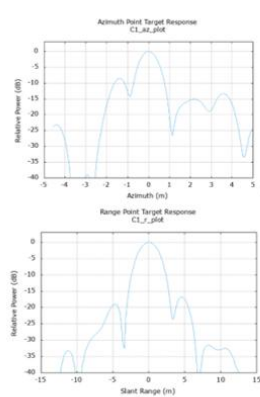
<b>Opportunistic Targets (OT)</b>	<b>Polarization</b>	<b>Range_3dB width</b>	<b>Azimuth_3dB width</b>	<b>SCR (in dB)</b>
<b>OT01 (363, 5799)</b>	VV	2.952	0.845	40.1827
<b>OT02 (341, 6043)</b>	VV	2.880	0.945	44.5314
<b>OT03 (318, 6293)</b>	VV	2.697	0.986	45.8941
<b>OT04 (595, 6231)</b>	VV	2.725	0.943	46.6587
<b>OT05 (286, 6477)</b>	VV	2.853	0.822	37.6775
<b>OT06 (578, 6490)</b>	VV	2.731	0.808	41.7496
<b>OT07 (258, 6682)</b>	VV	2.852	1.041	43.9584
<b>OT08 (549, 6732)</b>	VV	2.733	1.047	42.5240
<b>OT09 (507, 6865)</b>	VV	2.830	0.993	47.5683
<b>OT10 (204, 7138)</b>	VV	2.913	0.914	42.0526
<b>OT11 (473, 7112)</b>	VV	2.771	1.043	33.6091
<b>OT12 (730,7123)</b>	VV	2.786	0.958	46.7286

<b>OT13</b> <b>(179, 7414)</b>	VV	2.764	1.219	38.5753
<b>OT14</b> <b>(439, 7363)</b>	VV	2.767	0.919	41.9744
<b>OT15</b> <b>(155, 7693)</b>	VV	2.906	0.846	42.1335
<b>OT16</b> <b>(413, 7641)</b>	VV	2.850	0.877	43.5783
<b>OT17</b> <b>(305, 7867)</b>	VV	2.757	0.915	44.1853

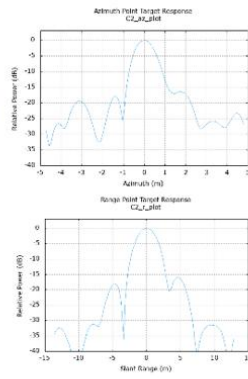
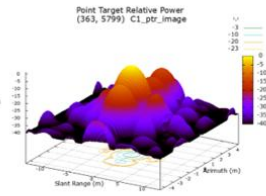
Clutter = 424, 6382

From the Table 11 we observed that the azimuth resolution is 0.84 meters and range resolution is 2.81 meters respectively which is approximately close to specified values.

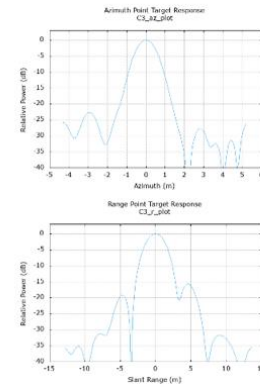
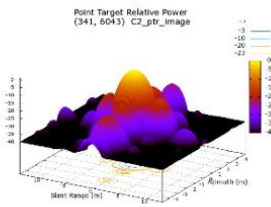
# Response functions for the windmills



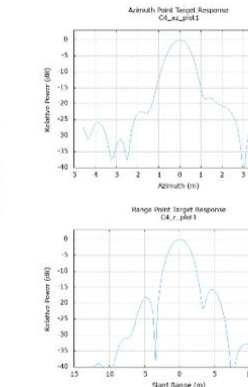
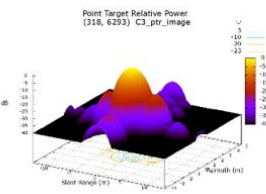
CR1



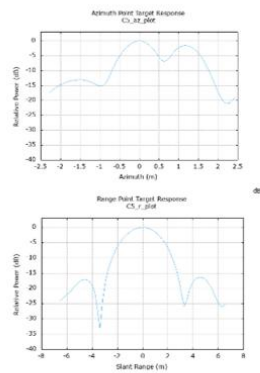
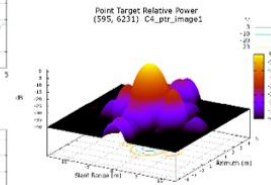
CR2



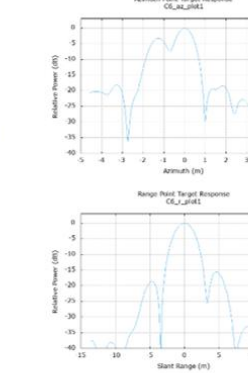
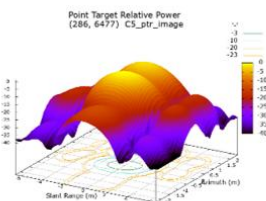
CR3



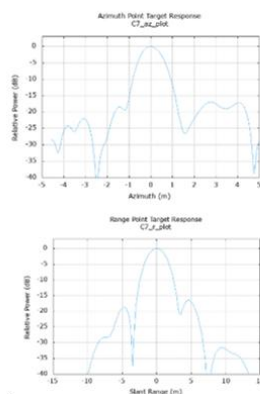
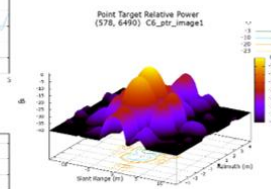
CR4



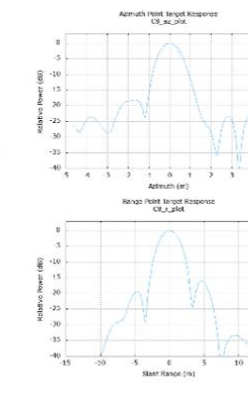
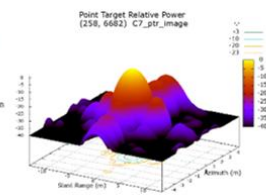
CR 5



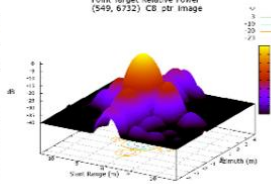
CR6

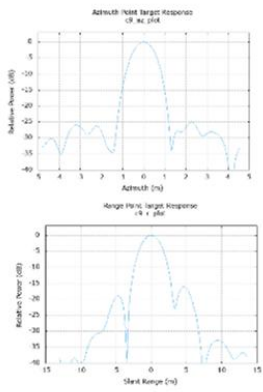


CR7

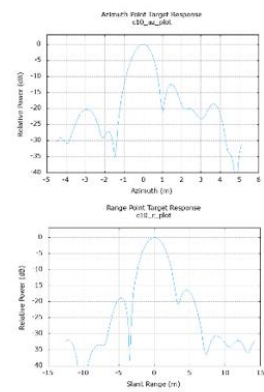
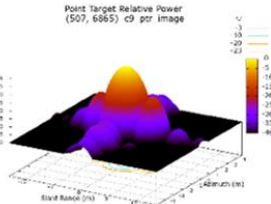


CR8

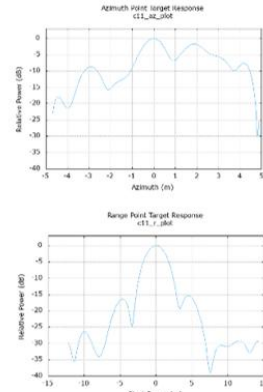
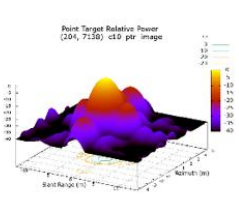




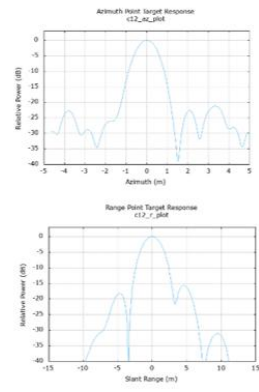
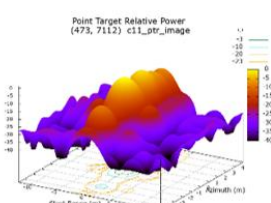
CR9



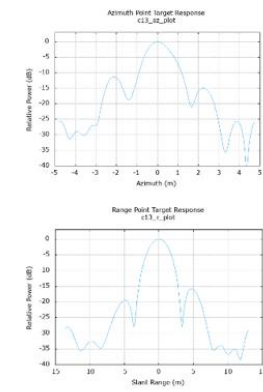
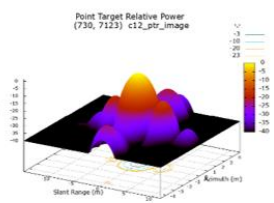
CR10



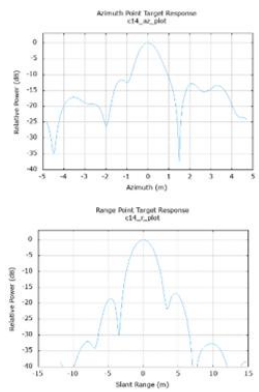
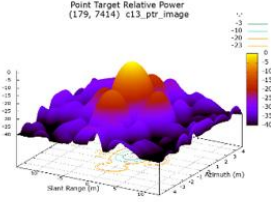
CR11



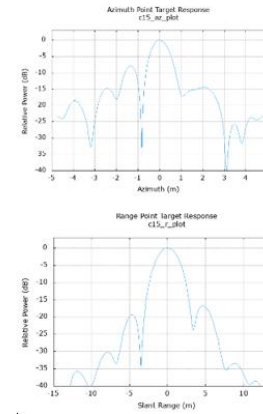
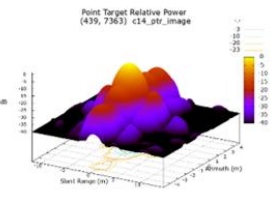
CR12



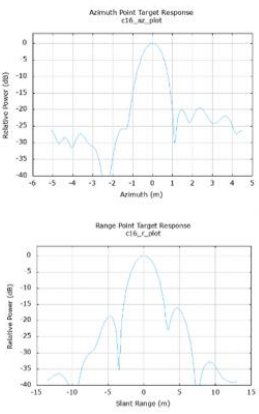
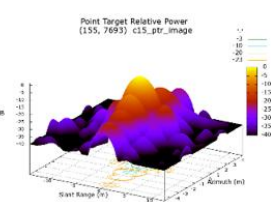
CR13



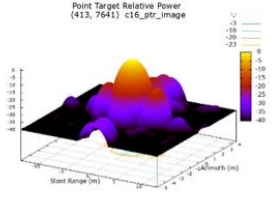
CR14

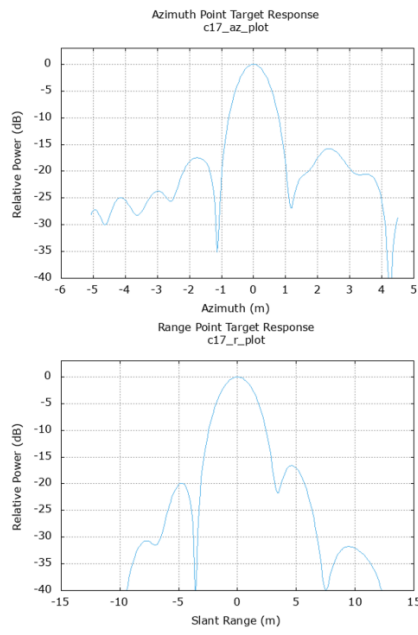


CR15



CR16





CR17

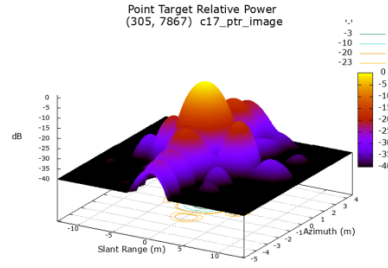


Figure 21. Impulse response function of windmills using SLC HH pol. data

## 7 SUMMARY AND CONCLUSIONS

Development of NASA-ISRO Dual frequency SweepSAR (NISAR) is under progress by ISRO in collaboration with Jet Propulsion Laboratory (JPL), NASA. It will provide S- and L-band space-borne SAR data with high repeat cycle, high resolution, and larger swath, with capability of full-polarimetric and Interferometric modes of operation. For the quantitative interpretation of images, acquired by SAR sensor, it is very much important to have properly calibrated data. Due to limited number of datasets available for ISRO's L&S airborne SAR mission (pre-cursor to NISAR), full-pol data of UAVSAR is used in this study to derive the polarimetric distortion matrix (PDM) and validate the results. In this study, evaluation of the radiometric and polarimetric calibration of full-pol L-band airborne SAR data using point targets and distributed target have been carried out. Analysis of the impulse response function of the point targets show that the estimated azimuth resolution ( $0.93 \pm 0.02$  meters) and range resolution ( $2.69 \pm 0.06$  meters) are close to the specified values. The difference between the estimated and provided calibration constant was found to be in the range of  $1 \text{ dB} \pm 0.45 \text{ dB}$  with a phase calibration error of  $1.58^\circ$ . Co-polarization channel imbalance (f) was found to be  $0.985 \pm 0.052$  (linear units), which is estimated using corner reflectors. While cross polarization channel imbalance (g) was calculated as 1.256 dB which is derived using featureless homogenous area (distributed target). The phase anomaly between cross channel of HV and VH polarization was found to be  $-2.07^\circ$ , which indicates that the phase error is high in receiving channel. The undulations present in the polarimetric signatures of co-pol and cross-pol after radiometric and phase correction, indicates that cross talk and channel imbalances are present. Polarimetric signature was also derived for point targets using polarimetric calibrated images and are shown in this report. Estimation of polarimetric distortion matrix (PDM) was done using advanced and robust Quegan's algorithm. Application of estimated PDM to the radiometrically and phase corrected dataset is in progress to validate the results. After the validation, this methodology will be utilized for the polarimetric calibration of L&S airborne SAR data and upcoming NISAR data.

## **ACKNOWLEDGEMENTS**

The authors gratefully acknowledge the encouragement and guidance received from Shri D K Das, Director-SAC. Authors express their sincere gratitude to Shri N M Desai, Associate Director, SAC, Ahmedabad for his support to carry out this activity. Thanks are also due to Deputy Director-EPISA, Dr. Raj Kumar for providing his critical comments for the improvement of the study. Authors would also like to thank Director-Nirma University, Dr. Alka Mahajan for her support throughout the study. Authors also thankfully acknowledge the cooperation and technical help received from Shri V M Ramanujam and Shri Raghav Mehra for this activity.

## **REFERENCES**

1. Abhisek, Maiti, Kumar Shashi, and Tolpekin Valentyn. "Polarimetric Calibration of SAR by using Man-made Point Targets and Uniformly Distributed Natural Targets." 2019.
2. Ainsworth, T.L., and Ferro-Famil. "Orientation angle preserving a posteriori polarimetric sar calibration." IEEE Transactions of Geoscience and Remote Sensing, 2006.
3. Alexander, G Fore, D Chapman Bruce, and P Hawkins Brian. *UAVSAR Polarimetric Calibration*. California: California Institute of Technology, 2014.
4. Chen, Xi, Wu Tao, and Zhong Xueliang. "Airborne Polarimetric SAR Experiments with Different Crosstalk Calibration Techniques." Chengdu: CIE InternationalConference on Radar- IEEE, 2011.
5. Freeman, A. *Radiometric caibration of SAR image Data*. California: Jet Propulsion Laboratory, California Institute of Technology, 1995.

6. Masanobu Shimda, Noriyuki Kawano, Manabu Watanabe, Takeshi Mottoka, and Masto Ohki. "Calibration and Validation of the PISAR -L2." JAPAN: Asia Pacific Conference on Synthetic Aperture Radar (AP SAR), 2013.
7. "Polarimetric Analysis of Airborne DLR-ESAR for Vegetation Characterization." Semantic Scholar, 2012.
8. Pottier, Eric, Jong Sen Lee, and Laurent Ferro Famil. "Advanced Concepts of Polarimetry." 2007. [earth.esa.int/landtraining07/polsar\\_advanced-concepts.pdf](http://earth.esa.int/landtraining07/polsar_advanced-concepts.pdf).
9. Quegan, Shaun. "A Unified Algorithm for Phase and Cross talk Calibration of Polarimetric Data-Theory and Observations." *Transactions on Geoscience and Remote Sensing, IEEE* 32, no. 1 (1994).
10. Ronald, J Muellerschoen, Chapin Elaine, and Alex Fore. *Recent Airborne SAR Calibration Results Using the Rosamond Array for P, L, and Ka-band Data*. CEOS SAR CAL VAL, 2015.
11. Shweta, Sharma, Dadhich Gautam, Rambhia Mihir, and K Mathur Alope. "Radiometric Calibration Stability Assessment for the RISAT-1 SAR Sensor using a Deployed Point Target Array at the Desalpar site, Rann of kutch, India." *International Journal of Remote Sensing*, 2017.